Scientific Contributions Oil & Gas, Vol. 48. No. 4, December: 433-462

SCIENTIFIC CONTRIBUTIONS OIL AND GAS

Testing Center for Oil and Gas
LEMIGAS

Journal Homepage:http://www.journal.lemigas.esdm.go.id
ISSN: 2089-3361, e-ISSN: 2541-0520

Comparative Analysis of Capacitance-Resistance Models and Machine Learning for CO_2-Eor Production Forecasting: A Case Study of Dynamic Connectivity in Heterogeneous Reservoir

Reyhan Rafsanjani[1], Agus Dahlia[1],Fajril Ambia[1], Novia Rita[1], Ayyi Husbani[1]

[1] Department of Petroleum Engineering, Faculty of Engineering, Universitas Islam Riau
113 Kaharuddin Nasution Street, Simpang Tiga, Pekanbaru, Riau, 28284, Indonesia

Corresponding Author : Reyhan Rafsanjani (reyhanrafsanjani@student.uir.ac.id)

Manuscript received: October 27th, 2025; Revised: November 17th, 2025
Approved: December 08th, 2025; Available online: December 30th, 2025; Published: December 30th, 2025.

ABSTRACT - This study evaluates an integrated forecasting framework that combines Capacitance-Resistance Models (CRMP and CRMIP) with ensemble machine learning algorithms (Random Forest and XGBoost) to predict CO_2-Enhanced Oil Recovery performance in the heterogeneous Volve Field. Reservoir simulation is performed using tNavigator with CO_2 injection at 941 tons/day (35 MMSCF/day) over 20 years. The results demonstrate the critical influence of CO_2-specific characteristics, with a determined Minimum Miscibility Pressure of 3299.68 psi and a corresponding oil Swelling Factor of 1.19. Machine learning models, particularly XGBoost, significantly outperformed conventional CRM methods, achieving exceptional accuracy (R^2 = 0.99-1.00, MAPE = 0.44 - 2.24%) compared to CRMP/CRMIP (R^2 = 0.55 - 0.72, MAPE = 16-23%). The CO_2 injection scenario substantially enhanced oil recovery, achieving a cumulative production of 15.73 MMSTB (RF 20.45%) compared to 9.38 MMSTB (RF 12.19%) for waterflooding, representing a 67.7% improvement and incremental recovery of 6.35 MMSTB. Interwell connectivity analysis reveales dynamic reservoir responses with time constants ranging from 916 to 927 days. The integration of physics-based models with non-linear machine learning algorithms significantly improves prediction accuracy while providing comprehensive insights into reservoir dynamics, allowing for optimal CCUS implementation in heterogeneous reservoir systems.

Keywords: CRMP, CRMIP, machine learning, DCA, CCUS.

How to cite this article:

Reyhan Rafsanjani, Agus Dahlia,Fajril Ambia, Novia Rita, Ayyi Husbani 2025, Comparative Analysis of Capacitance-Resistance Models and Machine Learning For Co2-Eor Production Forecasting: A Case Study of Dynamic Connectivity in Heterogeneous Reservoir, Scientific Contributions Oil and Gas, 48 (4) pp. 433-462. DOI org/10.29017/scog.v48i4.1930.

INTRODUCTION

The global energy transition has compelled nations to formulate strategies that can substantially reduce greenhouse gas emissions while maintaining long-term energy security. Within the oil and gas sector, carbon capture, utilization, and storage (CCUS) has emerged as a pivotal technological pathway in addressing these dual imperatives (Núñez-lópez & Moskal, 2019 (Qiao & Zhang 2025). The deployment of CO_2 as an injection agent in enhanced oil recovery (CO_2-EOR) offers a particularly compelling dual advantage: it enables the geological sequestration of anthropogenic CO_2 while simultaneously enhancing hydrocarbon recovery in mature reservoirs (Alam et al., 2022) (Núñez-lópez & Moskal 2019). The physicochemical properties of CO_2, including its high solubility in hydrocarbons and its ability to reduce oil viscosity, represent significant potential for improving displacement efficiency and mobilizing residual oil (Alam et al., 2022; Qiao & Zhang, 2025 and make CO_2-EOR a strategically important component of low-carbon reservoir management.

Despite these advantages, the performance of CO_2-EOR is profoundly influenced by reservoir heterogeneity (Jiashun Luo et al., 2022). Features such as preferential flow pathways, strong permeability contrasts, and non-uniform fluid distributions frequently lead to inefficient sweep and premature CO_2 breakthrough, reducing recovery performance (Alam et al., 2022 (Jiashun Luo, 2022. A substantial body of research has attempted to understand these behaviors through numerical reservoir simulations and waterflood performance analyses, including the use of capacitance-resistance models (CRM) to infer interwell connectivity.

Although CRM has demonstrated considerable utility during waterflooding operations, its prediction accuracy declines markedly under complex displacement regimes such as CO_2 flooding. In these environments, nonlinear system interactions and multiphase flow dynamics dominate and cannot be adequately captured by simplified analytical formulations. In contrast, machine learning methods have demonstrated strong capability in modeling nonlinear and high-dimensional behaviors (Du et al., 2024; Gao et al., 2023), but many existing studies have applied these techniques in isolation, thus sacrificing the physical interpretability that remains a critical strength of CRM-based approaches.

During the waterflooding phase, the present study employs a hybrid methodology that integrates CRM with decline curve analysis (DCA) to capitalize on the strengths of both approaches. CRM contributes insights into interwell connectivity and reservoir time constants, whereas DCA provides robust long-term production trend estimation. However, in transitioning to the CO_2 injection forecasting scenario, this hybrid configuration is no longer adopted. The fundamentally different flow behavior associated with CO_2 injection, characterized by miscibility effects, saturation evolution, and increased flow-path complexity, renders conventional decline behavior invalid and diminishes the relevance of DCA. Consequently, CRM is applied without hybridization, and machine learning models are introduced as complementary tools to capture the nonlinear and dynamic nature of CO_2-induced reservoir response (Gao et al., 2023).

To address these challenges, this study develops an integrated predictive framework that combines CRM, specifically, CRMP and CRMIP, with ensemble-based machine learning algorithms, namely Random Forest and XGBoost (Gao et al., 2023. CRM provides an interpretable, physics-informed representation of pressure propagation patterns and interwell connectivity, whereas machine learning contributes the capability to learn nonlinear dependencies inherent in CO_2 flooding processes (Du et al., 2024).

The use of long-term reservoir simulation data further enables rigorous calibration and validation of the predictive models (Emera & Kalantari Dahaghi, 2025, facilitating a detailed assessment of reservoir dynamic behavior, connectivity evolution, and incremental oil recovery potential under CO_2 injection. In summary, this study aims to establish a CO_2-EOR forecasting framework that delivers high predictive accuracy while preserving the physical interpretability essential for operational decision-making. Furthermore, the findings are expected to provide greater insights into the evolution of interwell connectivity, reservoir pressure response,

and recovery performance during CO_2 injection. The resulting contributions serve as a scientifically grounded reference for designing and optimizing CCUS implementation strategies in highly heterogeneous reservoirs, as well as advancing methodological development in contemporary reservoir forecasting.

METHODOLOGY

All data in this study were processed and analyzed using the tNavigator reservoir simulator to determine the injection flow rate and production flow rate. We used the Python programming language to create CRM and Machine Learning models, and evaluated the performance of these models using the$R^2$and MAPE.

Capacitance resistance model (CRM)

The mathematical model is known as the Capacitance Resistance Model (CRM) employs the principles of reservoir flow equations and material balance to predict the quantity of oil that will be released from the reservoir (De Holanda et al., 2018).

CRMP: producer-based representation

CRMP is a model that places producers at the center or focus of the model control system. In this scheme, production wells will be analyzed separately to achieve greater resolution (De Holanda et al., 2018. CRMP establishes a singular time constant (τj) for the drainage volume of each producer and a unique connectivity (f_ij) for each injection (i) and producer (j). Therefore, the continuity equation for producer j is expressed as follows:

$$\tau_j \frac{dq_j}{dt} + q_j(t) = \sum_{i=1}^{Ninj} f_{ij}\, i_i(t) - \tau_j J_j \frac{dp_{wf}^{(j)}}{dt} \qquad (1)$$

CRMIP: injector-producer based representation

CRMIP is the most recent CRM model to consider reservoir heterogeneity. Heterogeneity in this model means different individual/pair parameters, assuming a single value for all producers or reservoirs is unreliable (De Holanda et al., 2018). The Ordinary Differential Equation (ODE) for this pair-based volume control is written as follows:

$$\tau_{ij} \frac{dq_j}{dt} + q_{ij}(t) = f_{ij}\, i_i(t) - \tau_{ij} J_{ij} \frac{dp_{wf}^{(j)}}{dt} \qquad (2)$$

Decline curve analysis (DCA)

The two fundamental difficulties in appraisal work are determining a well's most probable future life and estimating its future production. The simplest and most readily available variable characteristic of a producing well is its production rate. Furthermore, the logical way to find an answer to the two problems mentioned above, by extrapolation, is to plot this variable production rate either against time or against cumulative production, extending the curves thus obtained to the economic limit (Arps, n.d.).

The CRM results for predicting this volatility model are not very good. To aid in better predicting how the flow rate would behave, CRM will be integrated with DCA. The model utilized in DCA is Exponential ARPs, which is as follows:

$$q = q_i e^{(-D_i \Delta t)} \qquad (2)$$

Machine Learning

Two ensemble learning algorithms are used as the main prediction. Random Forest is an advanced decision tree technique that can be applied for classification or regression. It also belongs to the ensemble learning family. A decision tree is an easy-to-use method because of its clear structure (Hidayat & Astsauri, 2021. XGBoost is considered the most powerful algorithm for building prediction models (Erfando & Khariszma, 2023. The data set is split into two parts: 80% for training and 20% for testing. The hyperparameters for both models are determined using techniques such as Grid Search and Random Search.

Integrated CCUS simulation

The sandstone reservoir selected for CO_2 injection has significant water content and a decline

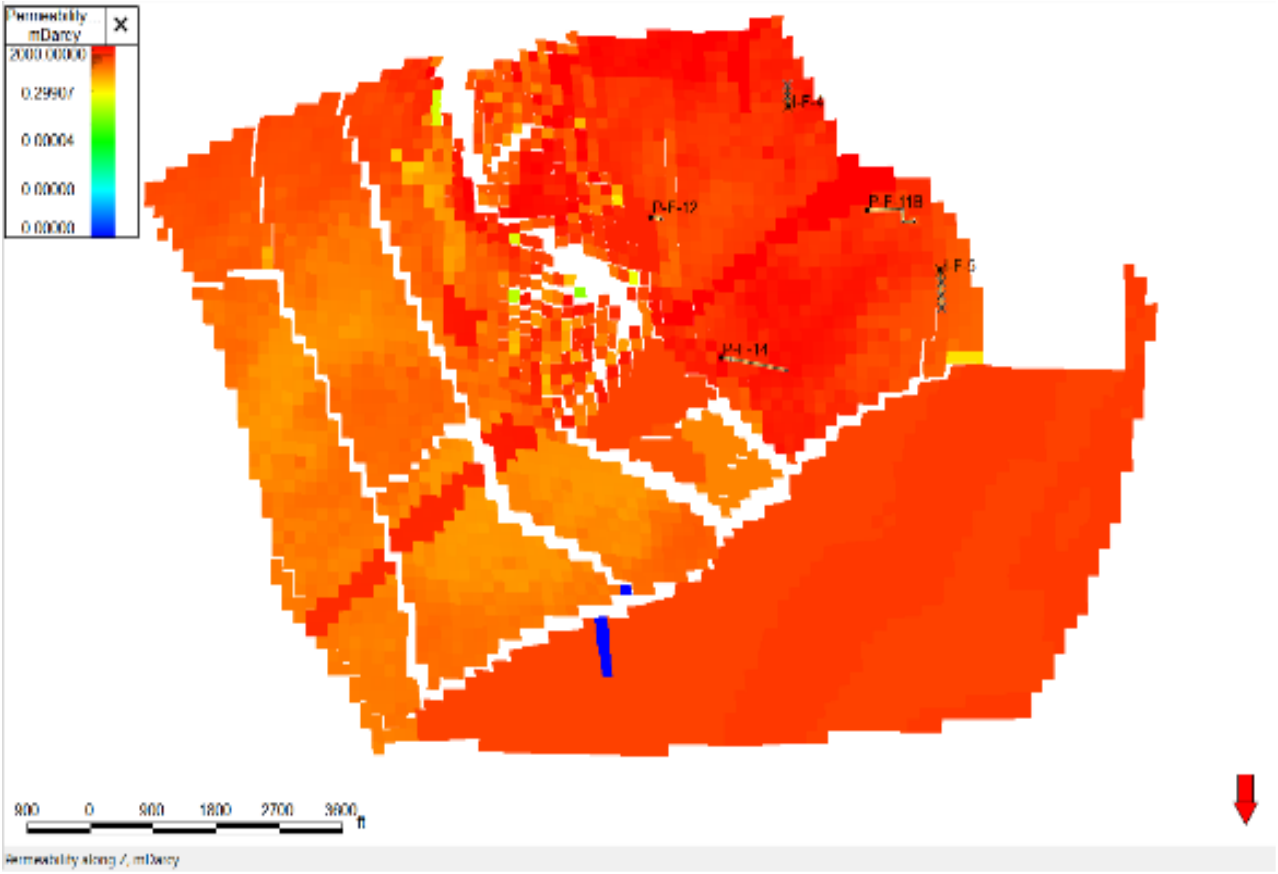

Figure 1. Permeability distribution on the volve field

in oil production rate during the water injection period in the secondary recovery phase. Therefore, tertiary recovery is required to increase the RF value with CO_2 injection. CO_2 injection selection is determined by fracture gradient, specifically utilizing an injection rate of 941 tons/day (35 MMSCF).

Reservoir simulations using tNavigator reveal MMP values in the field. This means that the injection rate remains constant and does not make the reservoir pressure similar to the BHP of the injection well. If the reservoir pressure equals the injection well's BHP, the injection rate decreases.

RESULTS AND DISCUSSION

In this study, the Volve field model was initialized and simulated using tNavigator, with the history matching process taking place between early 2015 and 2024. The water injection paradigm was modified to carbon dioxide (CO_2) injection, which was carried out for 20 years. Injection was continuous, and the flow rate was kept consistent by maintaining reservoir pressure, which differed from the pressure inside the well.

Table 1. Initialization of the volve field model

Parameters	Value	Unit
Original Oil in Place	76.9942	MMSTB
Original Water in Place	697.7655	MMSTB
Original Gas in Place	55.2871	MMSCF
Pore Volume	794.7169	Million RB

Figure 1 shows how the permeability distribution is represented. In general, the model's permeability distribution is very uneven.

The permeability values range from less than 1 mD (blue) to more than 1500 mD (bright red). The orange and red colors indicate that most of the reservoir region has good to very good permeability.

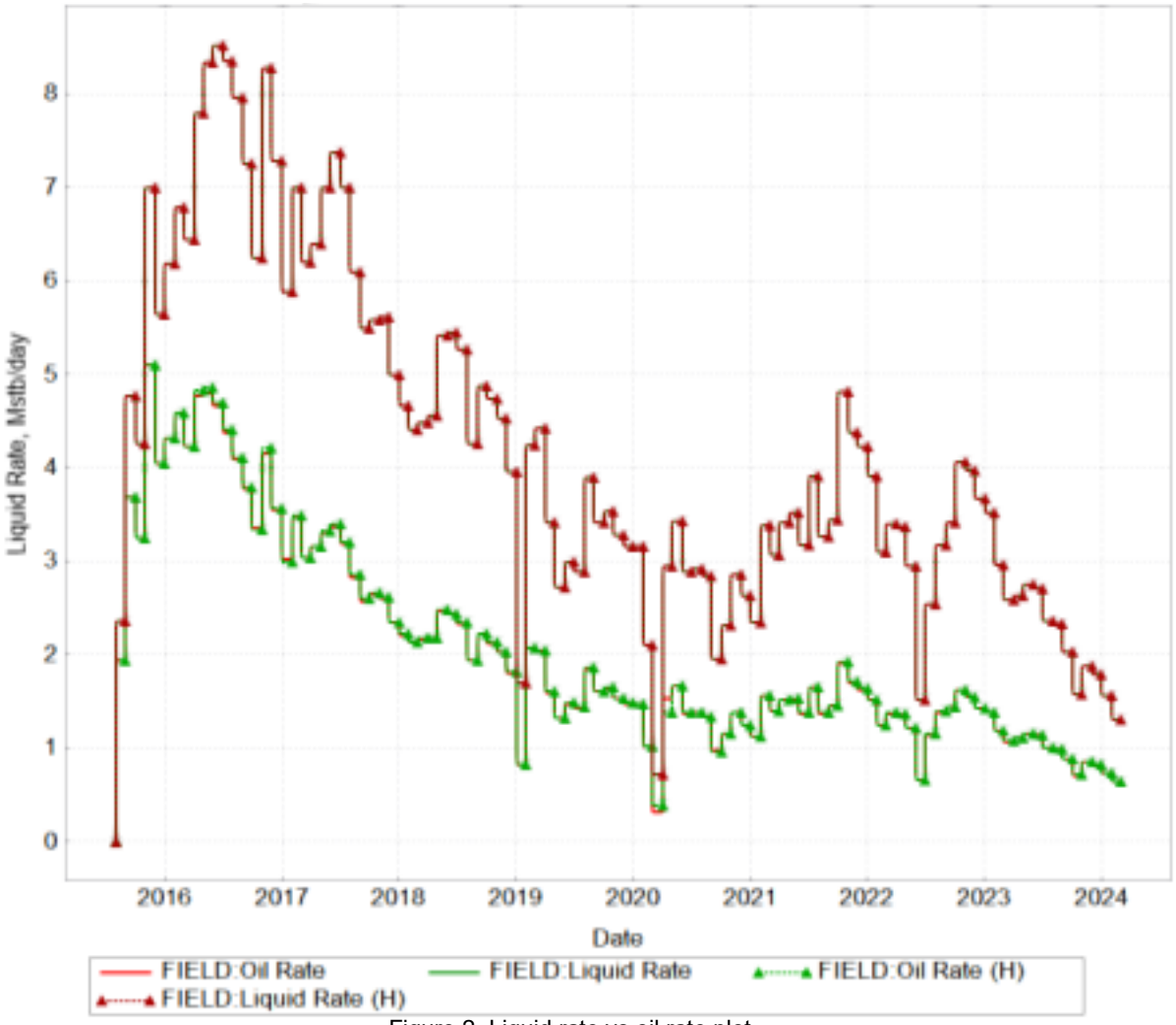

Figure 2. Liquid rate vs oil rate plot

The reservoir model was validated by modifying eight years of historical production data, with the results shown in Figure 2. There is a great visual match between the simulation results (solid line) and the historical data (markers), indicating that the model accurately depicts how the reservoir works.

Analysis History Matching and Validation Models, Hybrid CRM-DCA vs Machine Learning for Waterflooding.

To verify the accuracy of the model at each level, we compared the hybrid model predictions to actual production data from three main wells, as shown in Figure 3**.** In general, the model performed well in replicating complex and variable production behavior. This aligns with the research conducted by (Saraiva et al., 2014**,** which employed a multi-Hubbert model to forecast crude oil production in Brazil, effectively capturing production changes with considerable precision. The model's validity was quantitatively assessed using the Coefficient of Determination (R^2), which attained a value of 0.79, along with a low Mean Absolute Percentage Error (MAPE), signifying a robust correlation between the anticipated and actual data.

A high R2 value is a crucial measure of model reliability. This result is consistent with the forecasting model evaluation standards used in the oil and gas business, as applied by (Chavez-Rodriguez et al., 2015 in their analysis of Peruvian oil production.

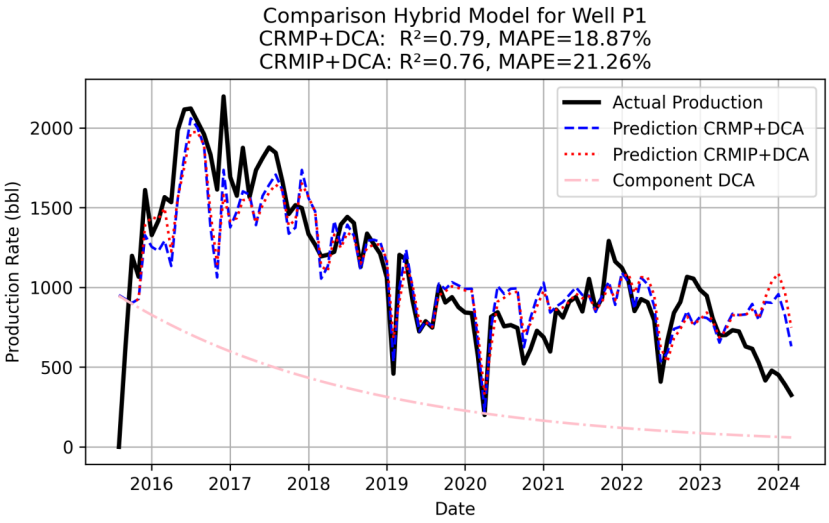

Figure 3 (a)

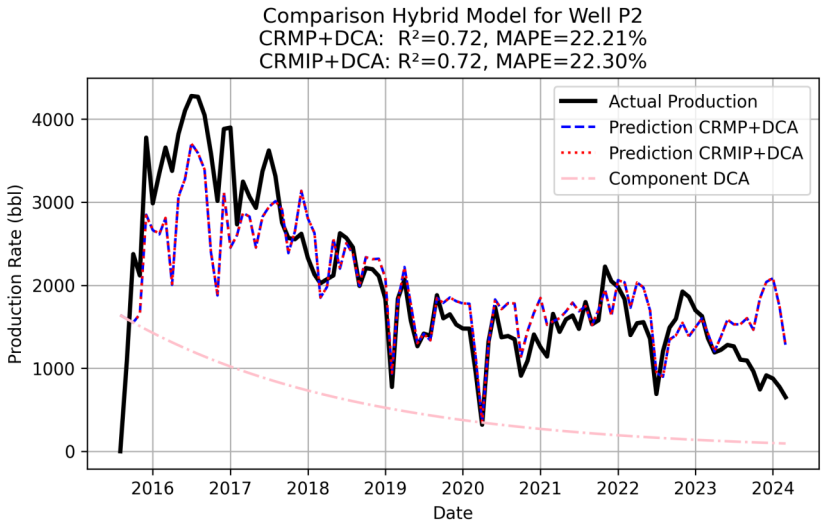

Figure 3 (b)

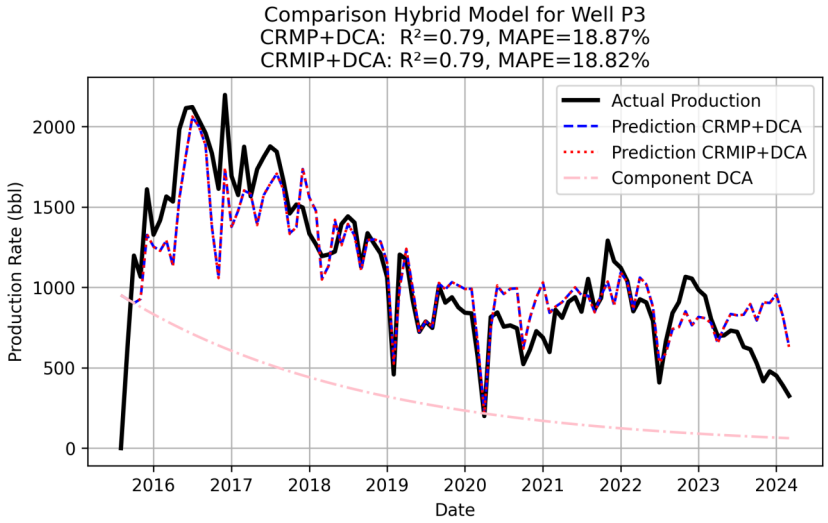

Figure 3 (c)

Figure 3. Plot comparison hybrid for well production (P1, P2, and P3)

Table 2. Interwell connectivity and time constant CRMP

Production well	Injection well		Time constant (τ) days
	I1	I2	
P1	0.0066	0.0098	30
P2	0.019	0.011	30
P3	0.0066	0.0098	30

Table 3. Interwell connectivity for CRMIP

Production well	Injection well	
	I1	I2
P1	0.0094	0.0064
P2	0.0191	0.0109
P3	0.0067	0.0099

Table 4. Time constant for CRMIP

Production well	Injection Well	
	I1	I2
P1	32	30.55
P2	30.86	30.54
P3	30	30

Table 2 shows the quantitative parameters of the CRMP model, offering a comprehensive understanding of the connection across wells in water injection operations (De Holanda et al., 2018. These results reveal that Injector_I1 has the biggest effect on production well P2 (f_ij 0.019), making it the injector-producer pair with the best connectivity (Shabani et al., 2020).

In contrast, Injector I2 offers higher pressure support for wells P1 and P3, highlighting reservoir variability and the intricacies of subsurface flow pathways (Salehian & Çýnar, 2019).

Table 3 shows all the parameters from the CRMIP model that can be used to find the unique time constants for each pair of injectors and producers. This method is consistent with the capacitance-resistance model methodology, which is effective in examining inter-well connections (Moreno & Lake, 2014).

Table 4 demonstrates substantial results, indicating that despite fluctuations, the time constant remained consistently within the range of 30-32 days. This relatively consistent time constant means that the reservoir's transmissibility and compressibility qualities are nearly identical throughout the research area (D. Wang et al., 2019).

Figure 4 shows that Injector_I1 is the most important injection well in this area, since it is closely connected to all three production wells (P1, P2, and P3). This means that Injector_I1 provides the highest pressure support in this area. In contrast, the majority of Injector_I2's connections go to well P1, giving it a more localized effect.

This connectivity map is a key part of making an effective injection plan and getting the most out of the sweep. According to (Ahmed 2007), the several ways that wells are connected directly affect the sweep pattern; hence, it is very important to understand this in order to optimize.

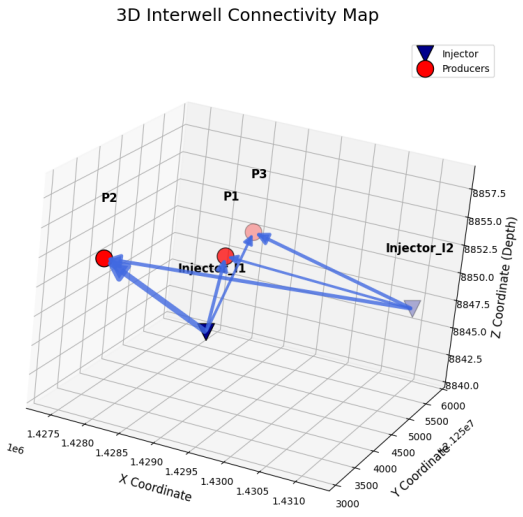

Figure 4. Interwell connectivity with 3D map

The results in Figure 5 show that both model variants (CRMP+DCA and CRMIP+DCA) function very well and are almost identical. This is evidenced by the consistently high Coefficient of Determination (R^2) values, ranging from 0.72 to 0.79, which means that the model is able to explain more than 72% of the variation in production data. In addition, the relatively low Mean Absolute Percentage Error (MAPE) value (below 23%) confirms that the model's prediction error rate is acceptable.

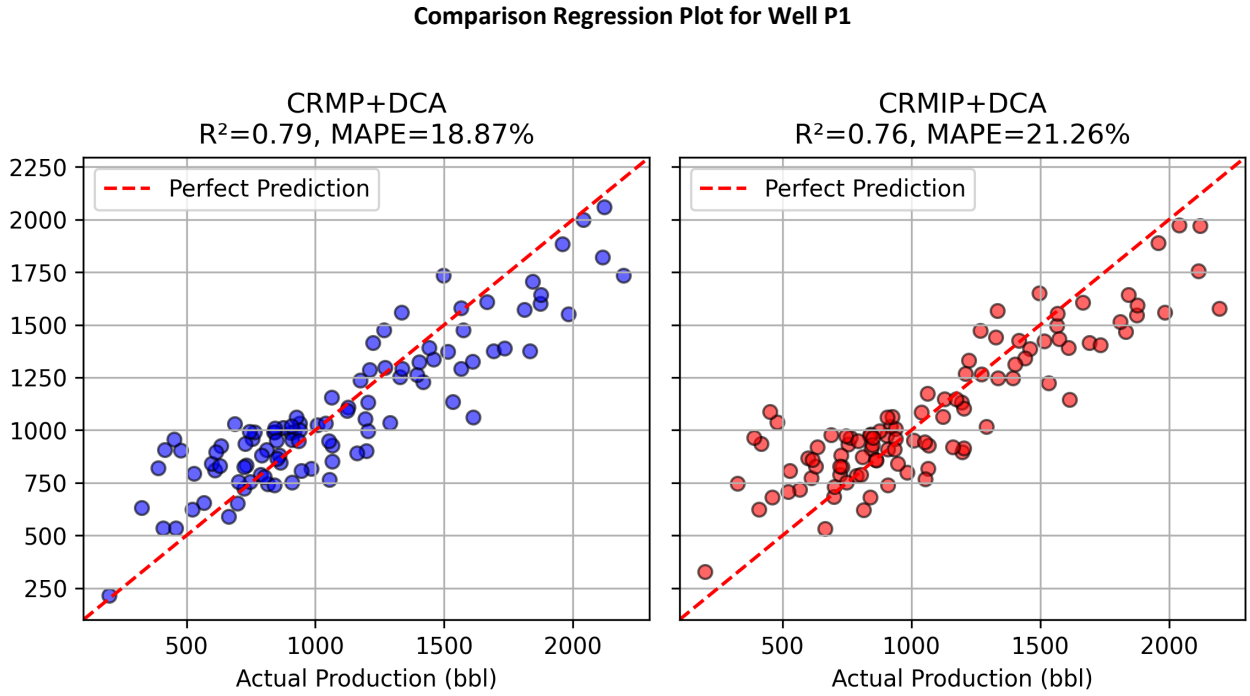

Figure 5 (a)

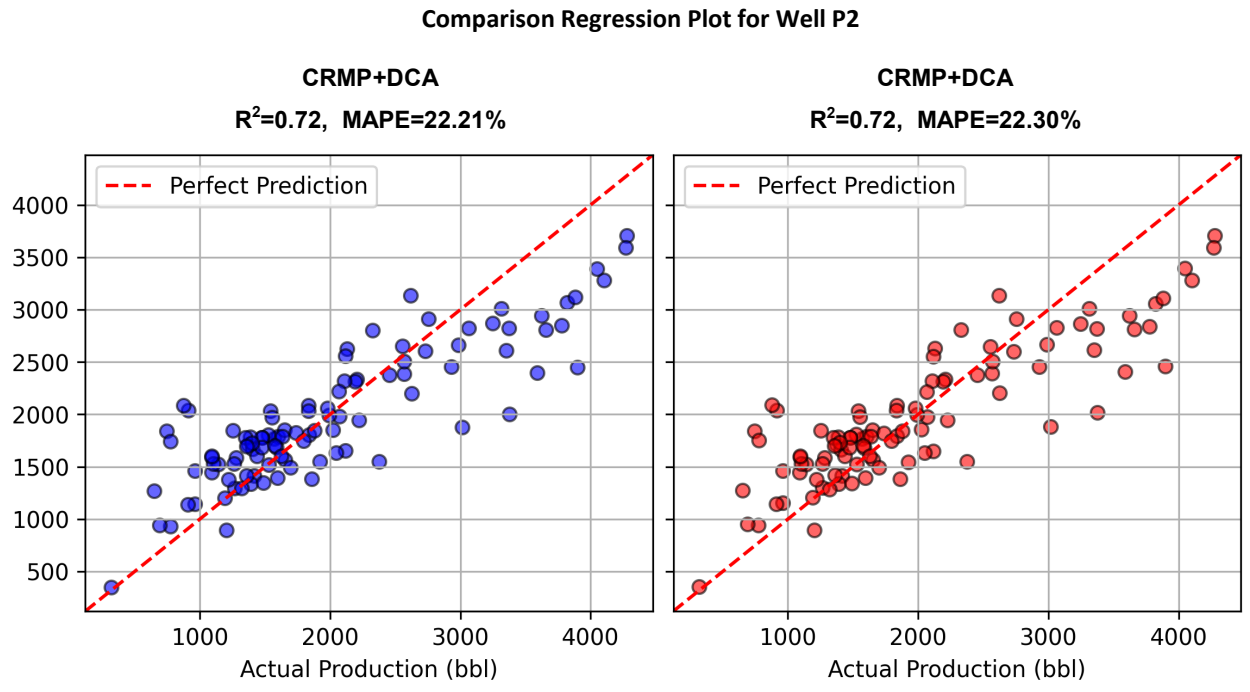

Figure 5 (b)

In general, this regression graph provides strong statistical evidence that the hybrid model developed can accurately predict things at the level of single wells. This result corroborates the studies conducted by Chicco et al (2021) which underscores that R^2 is a more relevant and dependable metric than MAPE for assessing regression model performance, particularly in scientific and industrial settings.

Figure 6 displays the results of the performance study of the Random Forest model based on machine learning. The model accurately predicts production rates, with an R^2 value of 0.98 and an MAPE of approximately 6%. This performance is similar to other studies demonstrating the efficacy of Random Forest in predicting reservoir parameters, as evidenced by (Rhamadhani et al., 2023, who attained an R^2 of 0.974 for oil production forecasting.

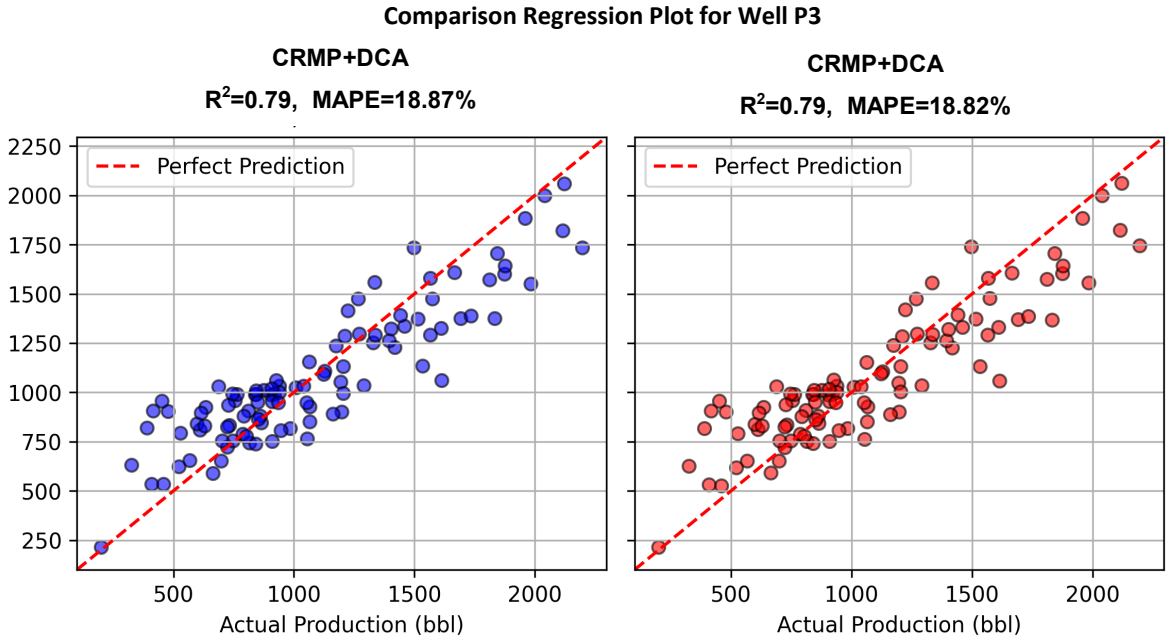

Figure 5 (c)
Figure 5. Comparison Regression Plot for Well Production (P1, P2, and P3)

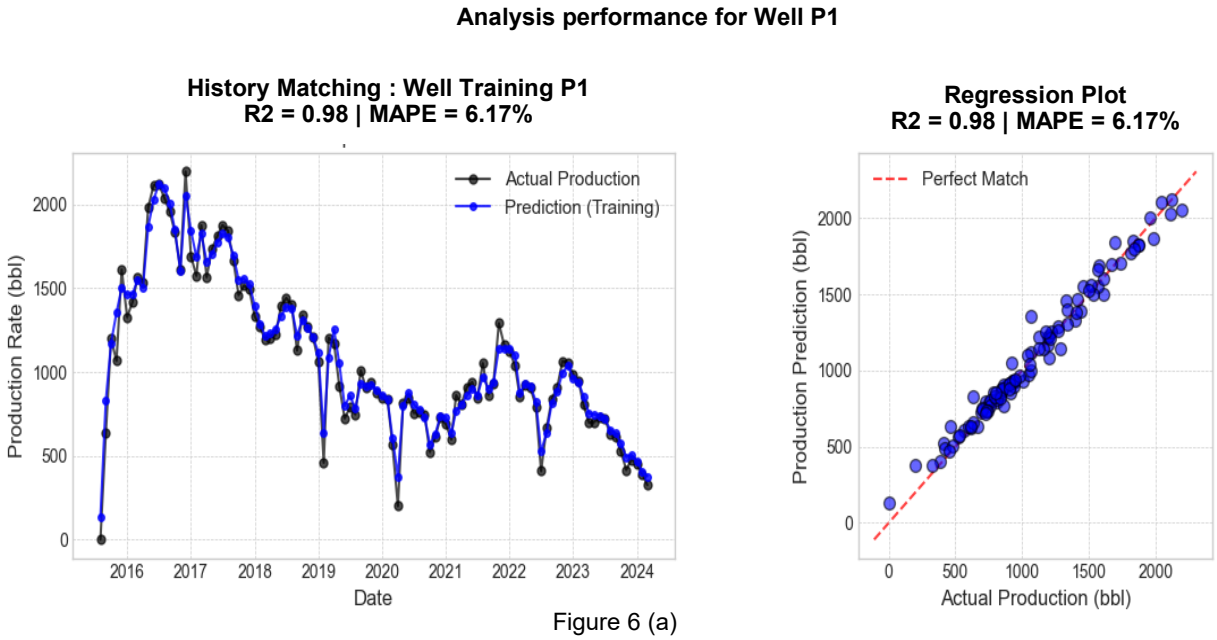

Figure 6 (a)

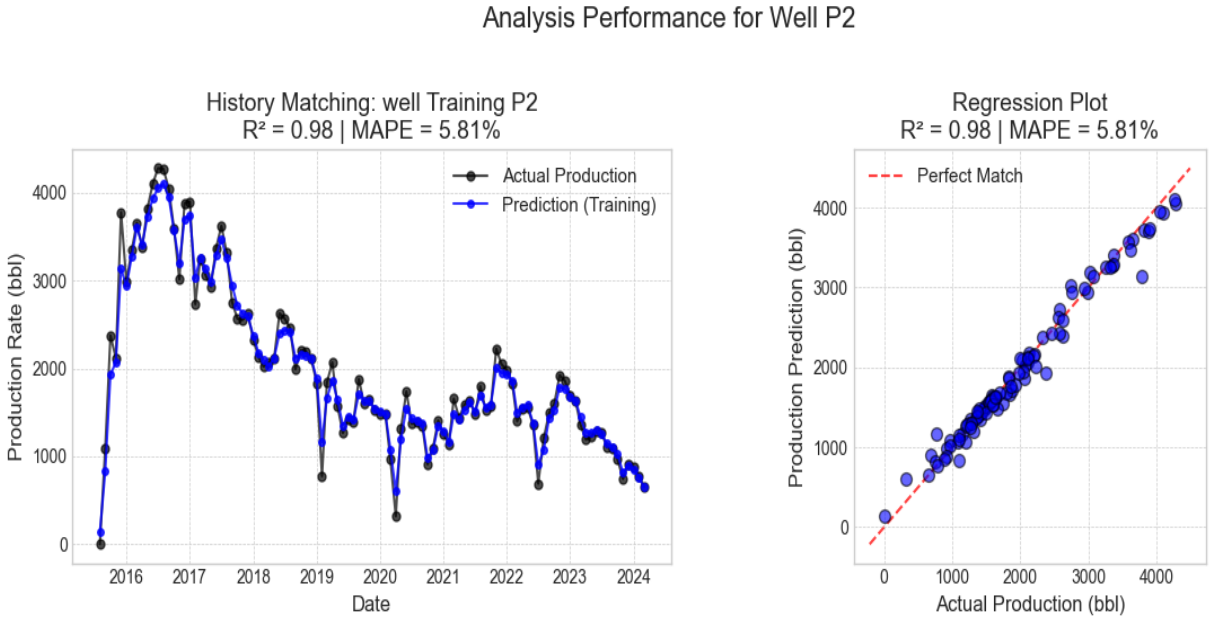

Figure 6 (b)

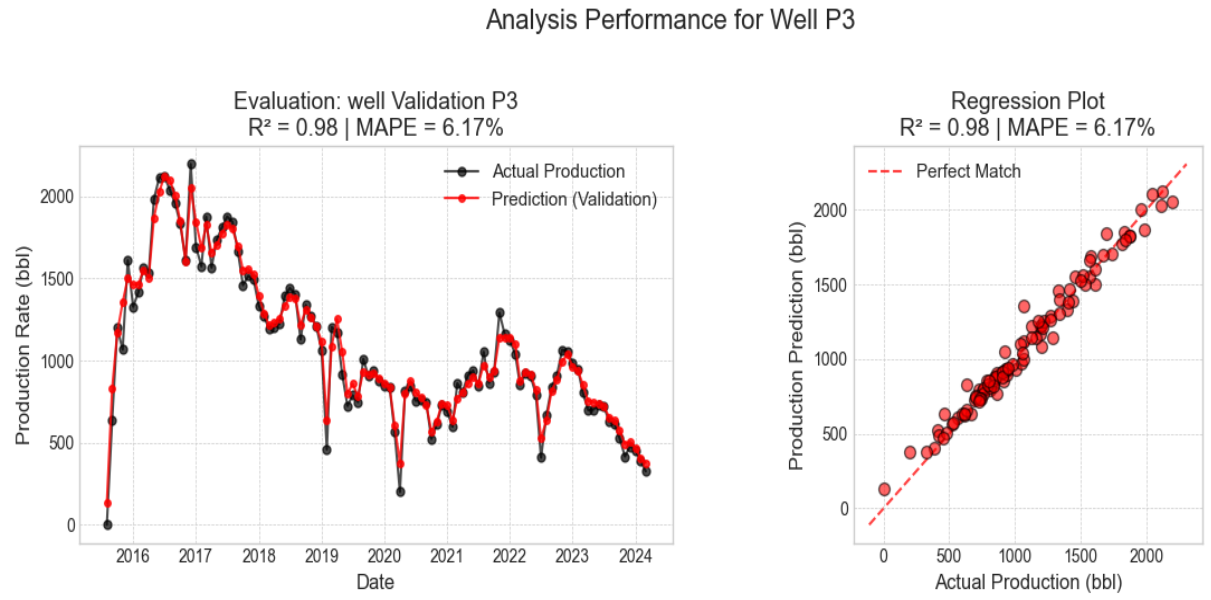

Figure 6 (c)
Figure 6. Analysis Random Forest for Well Production (P1, P2, and P3)

The most important part of this analysis is how well the model works on both the training data (Wells P1 and P2) and validation data (Well P3). The model's ability to produce accurate predictions on previously unseen data suggests that it is not overfit and has good generalizability. According to the author, machine learning methods can improve predictions with an R^2 close to 0.80.

Figure 7 shows the data used for training (Wells P1 and P2). The XGBoost model fit quite flawlessly, with a Coefficient of Determination (R^2) = 1.00 and a Mean Absolute Percentage Error (MAPE) of less than 0.6%. This excellent result is consistent with what other studies' findings about XGBoost's potential to be very accurate. However, the true validation lies in the model's performance on previously unseen data. On the validation data (Well P3), the model was able to maintain its outstanding performance with $R^2 = 0.99$ and MAPE = 0.86%. This very high consistency in performance between the training and validation data

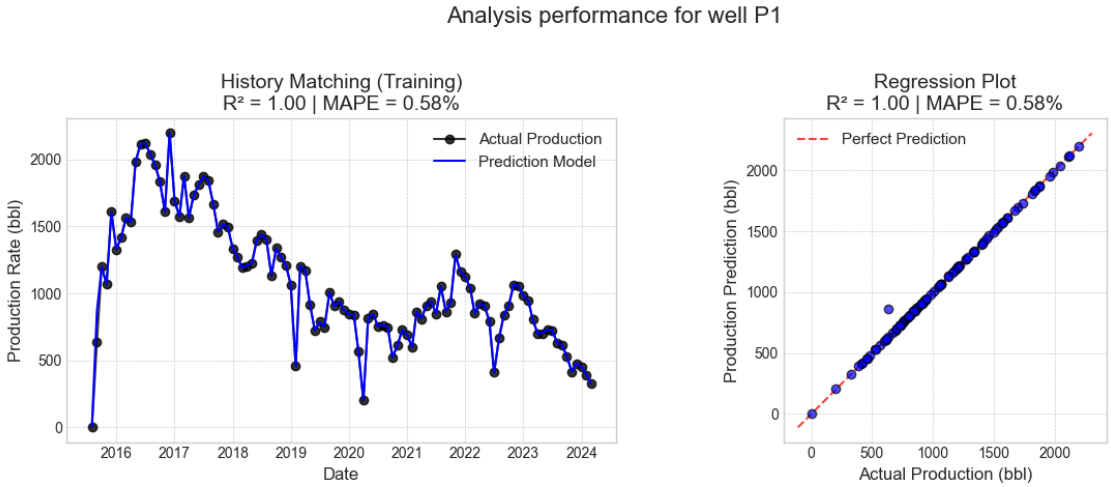

Figure 7 (a)

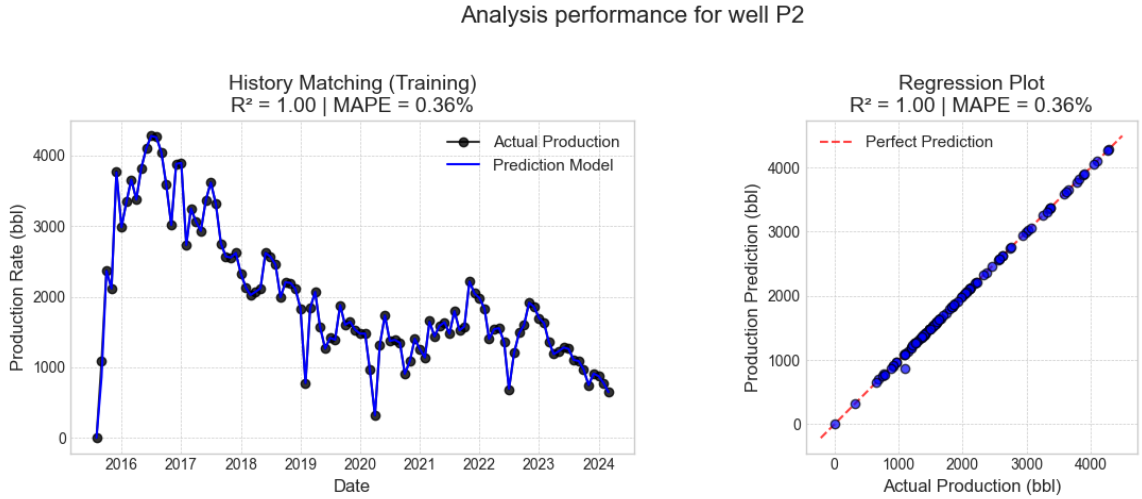

Figure 7 (b)

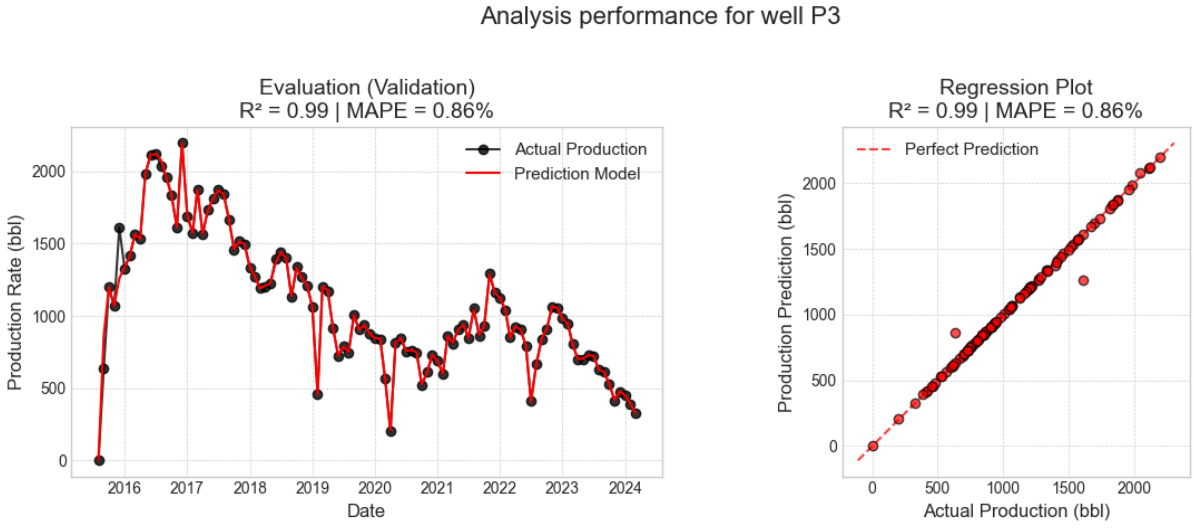

Figure 7 (c)
Figure 7. Analysis XGBoost for Well Production (P1, P2, dan P3)

convincingly proves that the model is not overfit and has very strong generalization capabilities. This finding is corroborated by (Fajrul Haqqi et al., 2023, who found that variations in XGBoost training and testing exhibited no signs of overfitting, and by (Asnawi et al., 2024, who validated that the XGBoost model showed no systematic bias, with prediction errors evenly distributed. The regression graph displays data points grouped in an almost perfect straight line, indicating that this XGBoost model is accurate and reliable enough to predict production. This advantage is in line with the many successful applications of XGBoost in various situations.

Forecast for CO_2 injection

The liquid-volume versus pressure plot, Figure 8, provides direct quantification of a key CO_2-EOR mechanism: oil swelling due to CO_2 dissolution. At the constant reservoir temperature of 224.6°F, the curve exhibits a characteristic hump. The initial oil volume at high pressure (~4000 psi) is approximately 1.05 RB. As pressure decreases into the miscible region near the defined MMP of 3299.68 psi, the volume swells to a maximum of 1.25 RB. The ratio of these volumes defines the Swelling Factor = 1.19, confirming that the oil undergoes a 19% volumetric expansion. This physical swelling exerts an internal driving force that helps mobilize residual oil by reducing capillary trapping and lowering residual oil saturation (Sugihardjo 2009).

This quantified mechanism has important field implications: while it underpins the substantial incremental recovery (6.35 MMSTB), its pressure-dependent nature also explains the uneven sweep efficiency observed in the simulation. Optimal swelling and recovery occur only in areas where pressure remains above the MMP, inherently amplifying the effects of reservoir heterogeneity and resulting in the channeling and early breakthrough patterns visualized in Figures 14 and 15.

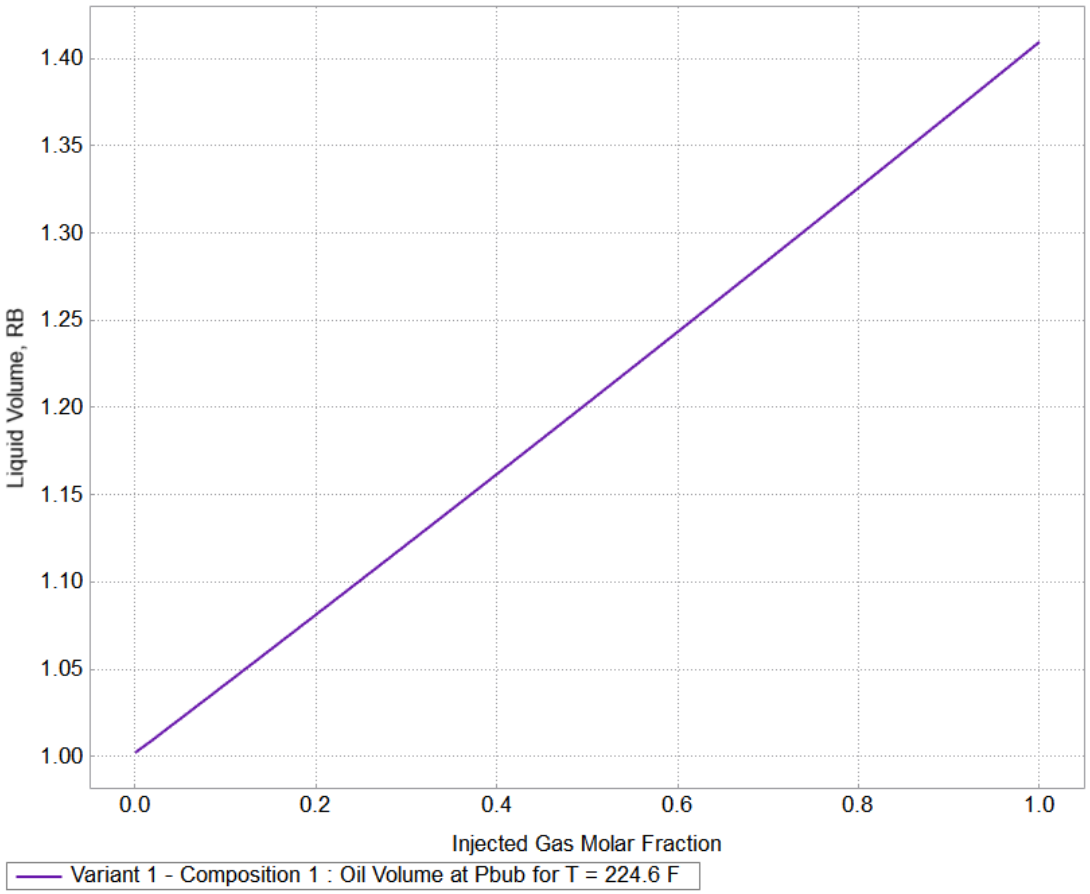

Figure 8. CO_2 induced oil swelling behavior at reservoir temperature (224.6°F)

Figure 9 shows the concentration of CO_2 in the oil phase as a function of pressure for the Volve Field fluid composition. The inflection point (or sharp increase) in the curve, indicated by the vertical dashed line, defines the MMP at 3299.68 psi. Pressures above this threshold enable first-contact or multi-contact miscibility, leading to a significant reduction in interfacial tension and oil saturation residual—the core mechanism driving the enhanced recovery in the forecasted CO_2-EOR scenario (Sugihardjo 2009).

The physical and chemical characteristics of CO_2 differ from those of water, influencing displacement mechanisms and sweep efficiency during EOR operations. Unlike water, CO_2 exhibits miscibility with crude oil above the Minimum Miscibility Pressure (MMP), reducing interfacial tension and oil viscosity and enhancing microscopic displacement efficiency. Furthermore, CO_2 dissolution induces oil swelling, as quantified by the Swelling Factor of 1.19, which further mobilizes residual oil. However, the higher mobility of CO_2 relative to oil and water typically leads to unfavorable mobility ratios, promoting viscous fingering and early breakthrough—phenomena not observed in waterflooding. These characteristics necessitate different operational strategies, such as WAG (Water-Alternating-Gas) injection or mobility control agents, to mitigate channeling and improve volumetric sweep in heterogeneous formations (Sugihardjo 2009).

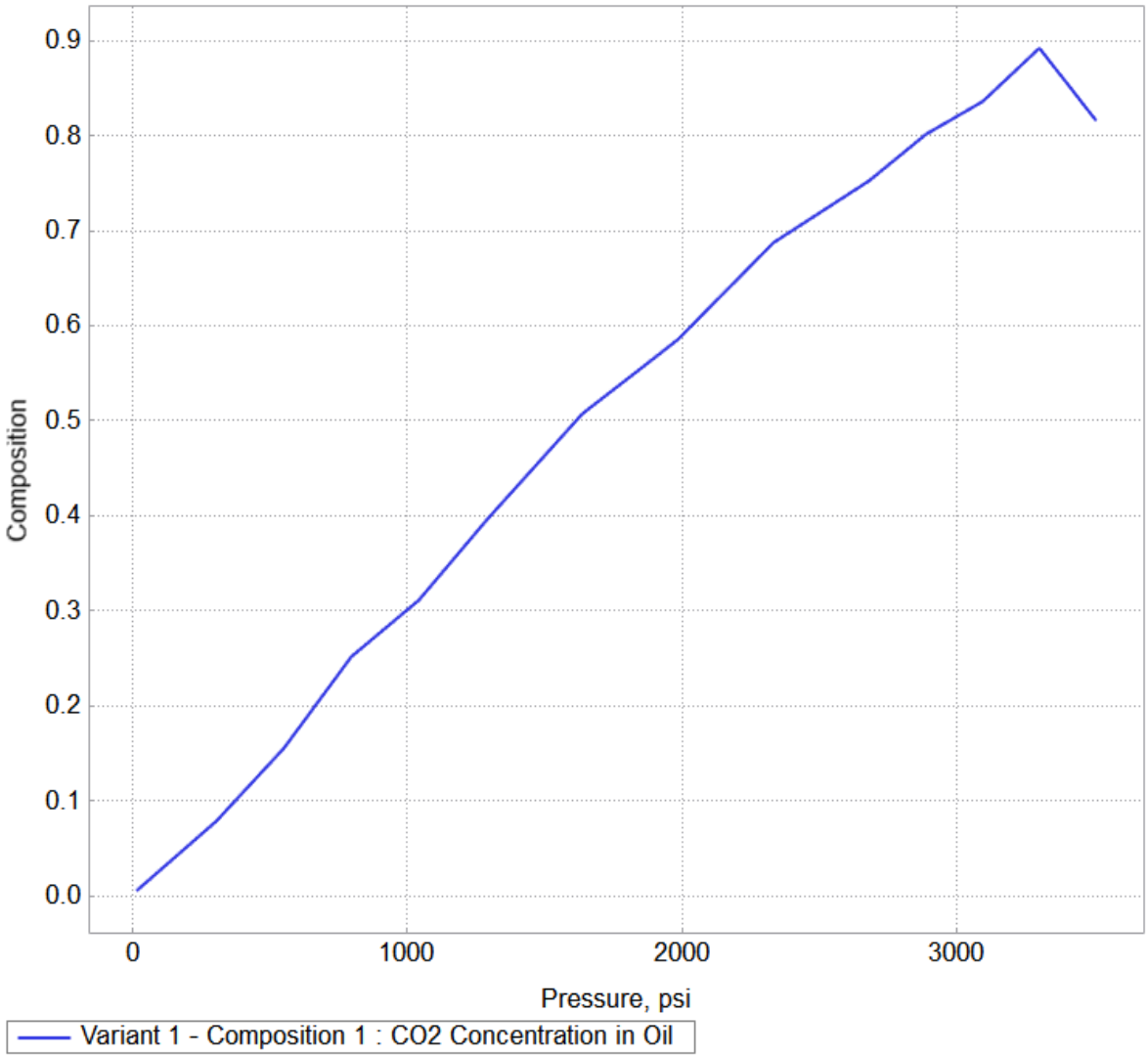

Figure 9. Determination of minimum miscibility pressure (MMP)

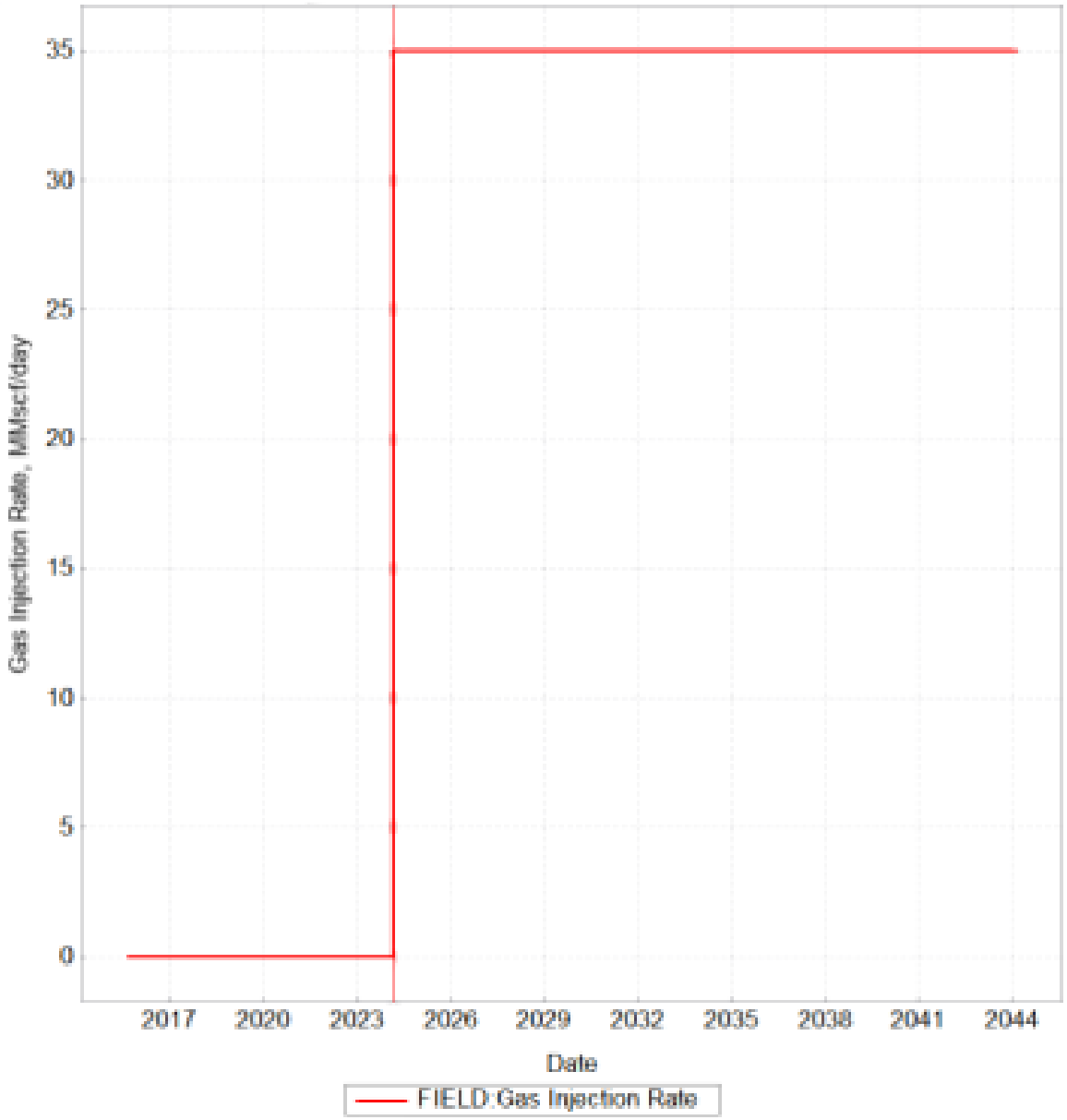

Figure 10. Injection rates of CO□ for 2 wells of injection

Figure 10 shows the gas injection scenario for reservoir performance forecasting. Waterflooding before 2025, followed by a constant rate of 941 tons/day (35 MMSCF) beginning in early 2025 and lasting 20 years until 2044.

This stable rate control scenario simulates gas flooding impacts on oil production enhancement and reservoir pressure maintenance (Orin et al., 2025). The approach enables comprehensive evaluation of enhanced oil recovery through controlled, long-term gas injection simulation (Khurshid & Afgan 2021).

The forecasting results demonstrate the effectiveness of gas injection EOR initiated in early 2025. Total field production was successfully stabilized at high levels, proving the gas injection scenario's success (Kristanto et al., 2025). Well P-F -12 (P2) shows significant improvement with stable production at 550 STB/day, while wells P-F-11B (P1) and P-F-14 (P3) continue declining. This contrasted response confirms reservoir heterogeneity and uneven gas sweep efficiency (Ramadhan et al., 2023). The injected gas flows through preferential pathways to P-F-12, while other well areas lack adequate pressure support (Shafiei et al., 2024).

Figure 12 effectively quantifies the benefits of implementing CO_2 injection projects compared to continuing existing Waterflooding scenarios. This approach is supported by research demonstrating that CO_2 injection significantly enhances oil recovery compared to conventional Waterflooding methods (Alam et al., 2022). The graph indicates that after 2025, the CO_2 injection scenario (orange) results in significantly higher daily production rates, as evidenced by the steeper slope of its curve.

This improvement aligns with studies demonstrating that CO_2 injection can achieve oil recovery rates of 68-73% of original oil-in-place, substantially outperforming conventional Waterflooding (Alam et al., 2022). While the continued Waterflooding scenario (red) would only reach a total cumulative production of approximately 9.38 MMstb, the CO_2 injection scenario is projected to reach 15.73 MMstb over the same period.

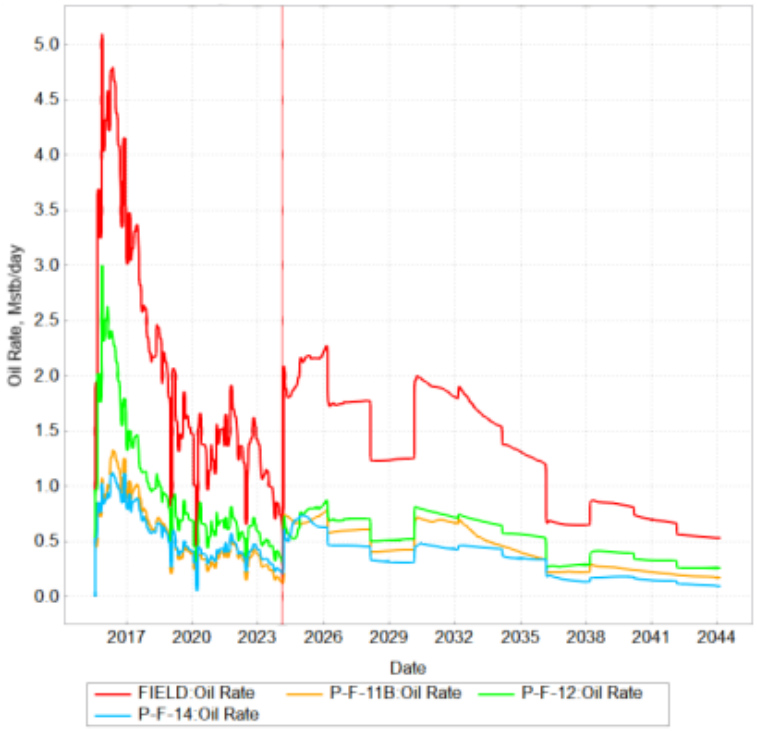

Figure 11. Oil rates for the field and 3-well Producers

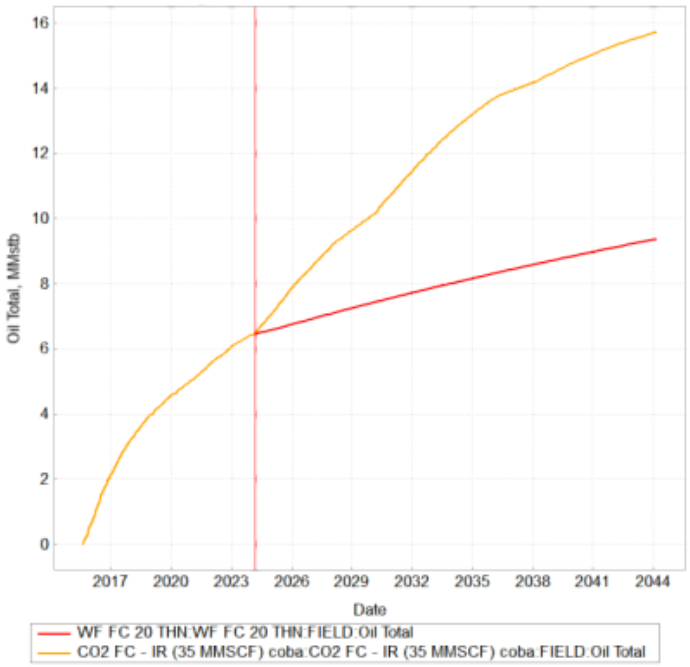

Figure 12. Oil Total during CO_2 Injection and Waterflooding

Figure 13 shows the field average pressure profile, which clearly illustrates three phases: initial depletion until 2024, followed by very rapid re-pressurization due to injection, and ending with a new long-term decline phase. This profile demonstrates that while the intervention scenario successfully and significantly increased reservoir energy initially, it was insufficient to maintain pressure permanently over the course of production time.

This three-phase pressure behavior is supported by research findings, which revealed that injection strategies can effectively restore reservoir pressure in the short term (S. Lee et al., 2023), and rapid pressure restoration can occur following hydraulic stimulation (S. Lee et al., 2023).

Figure 14 shows the final oil saturation map that visually demonstrates the presence of uneven sweep efficiency. Zones with low oil saturation (blue/green) indicate areas successfully swept by gas injection, particularly around the injector and toward well P-F-12. However, extensive areas with high oil saturation (yellow/orange) show significant bypassed oil volumes, highlighting the impact of reservoir heterogeneity on EOR project performance (Ramadhan et al., 2023)

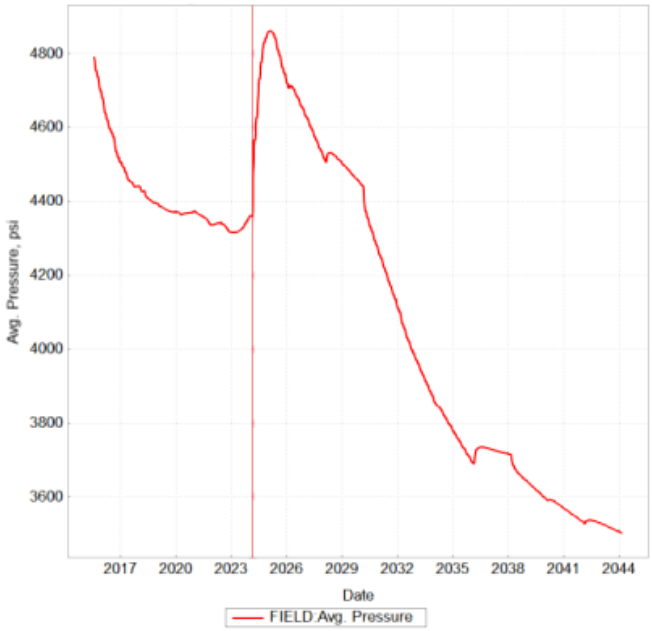

Figure 13. Reservoir pressure of the end CO_2 injection

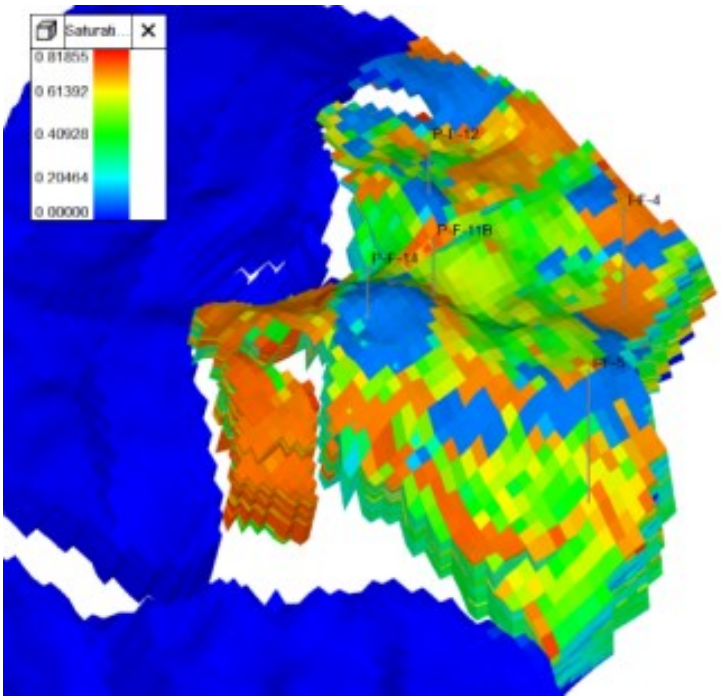

Figure 14. Oil saturation of the end simulation CO_2 injection

This visualization effectively illustrates how reservoir heterogeneity causes preferential flow paths during gas injection, resulting in incomplete oil displacement (Fang et al., 2024. The heterogeneous reservoir with different permeability zones leads to varying sweep efficiency, where some areas experience effective fluid displacement while others remain largely untouched, demonstrating the fundamental challenge of achieving uniform oil recovery in complex geological formations (Telmadarreie & Trivedi 2020).

Figure 15 illustrates highly non-uniform CO_2 breakthrough profiles among production wells, indicating reservoir heterogeneity. Wells P-F-14 (green) and P-F-12 (orange) exhibit very rapid and large breakthroughs, indicating the presence of thief zones that reduce injection efficiency. Meanwhile, well P-F-11B (red) remains mostly unchanged, indicating very poor connectivity. This data is crucial for evaluating uneven CO_2 sweep efficiency (Fang et al., 2024).

High reservoir heterogeneity can lead to early CO_2 breakout and flooding, particularly as the standard deviation increases, resulting in small sweep regions. Gas channeling and low sweep efficiency are common challenges in highly heterogeneous reservoirs (Fang et al., 2024).

Table 5. Compare Waterflooding vs CO_2 Injection

Scenario	Oil cumulative (MMSTB)	RF %
Waterflooding	9.38	12.19
CO_2 Injection	15.73	20.45

Table 5 concisely compares the final results of the two development scenarios. The results definitively demonstrate that the CO2 injection scenario is far superior, with total cumulative oil production reaching MMSTB (RF 20.45%) compared to Waterflooding, which only achieved 9.38 MMSTB (RF 12.19%). The implementation of this EOR project successfully provided an incremental oil recovery of 6.35 MMSTB.

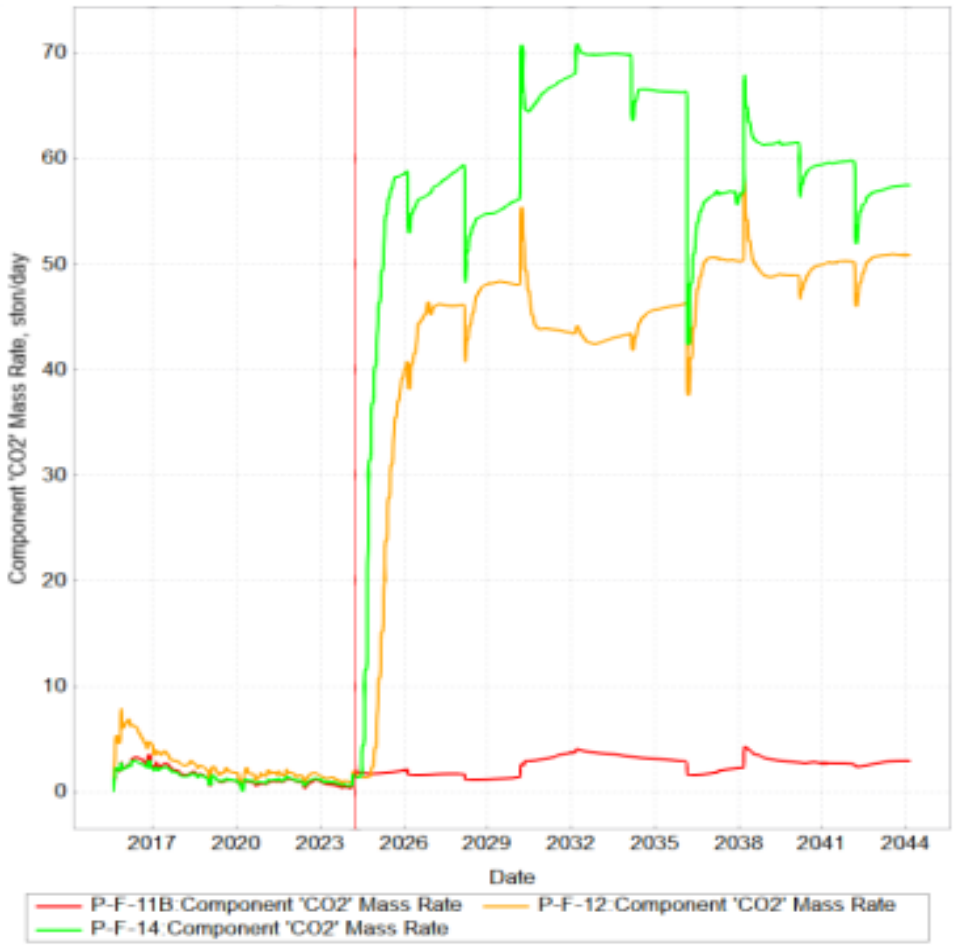

Figure 15. Production CO_2 mass rate

Analysis history matching and validation models, CRM vs machine learning after forecast CO_2 injection

Figure 16 shows the production rate prediction results for wells P1, P2, and P3 using the Capacitance Resistance Model (CRMP) and Capacitance Resistance Model with Injection Producers (CRMIP) methods for the 2024-2045 time periods.

Well, P1 demonstrates the best prediction performance with R^2 values of 0.722 and MAPE of 16.1% for both models, indicating good accuracy in capturing the production decline trend from ~2000 bbl/day to ~600 bbl/day. Meanwhile, wells P2 and P3 exhibit lower prediction performance with R^2 around 0.55 and MAPE ~23%, showing challenges in modeling more complex production fluctuations in both wells (Fu et al., 2022).

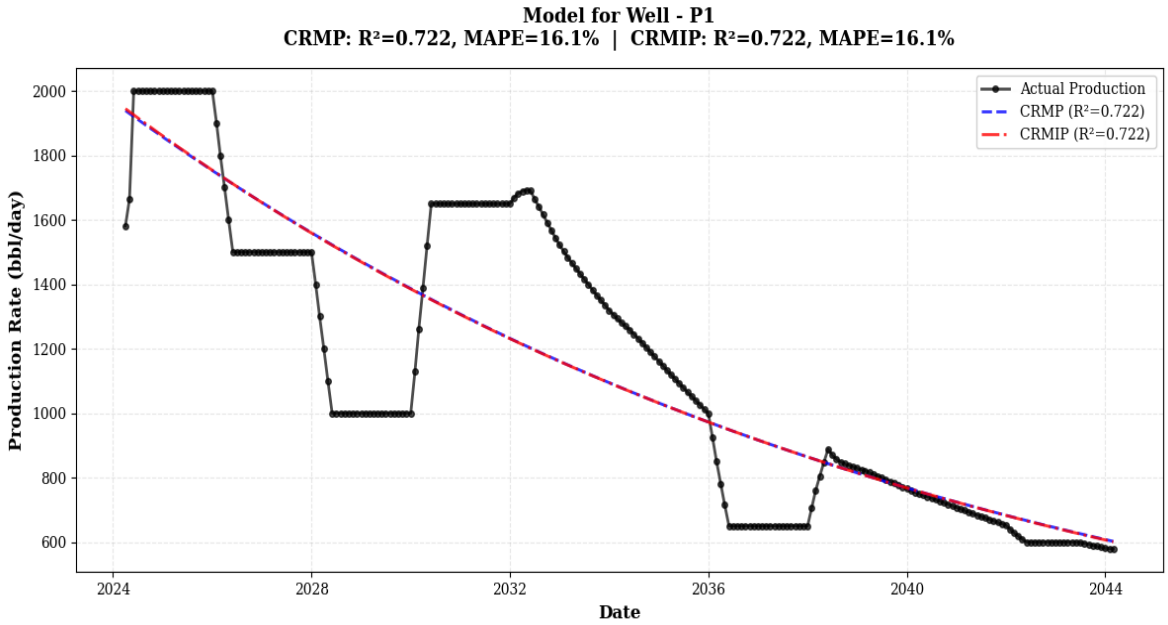

Figure 16 (a)

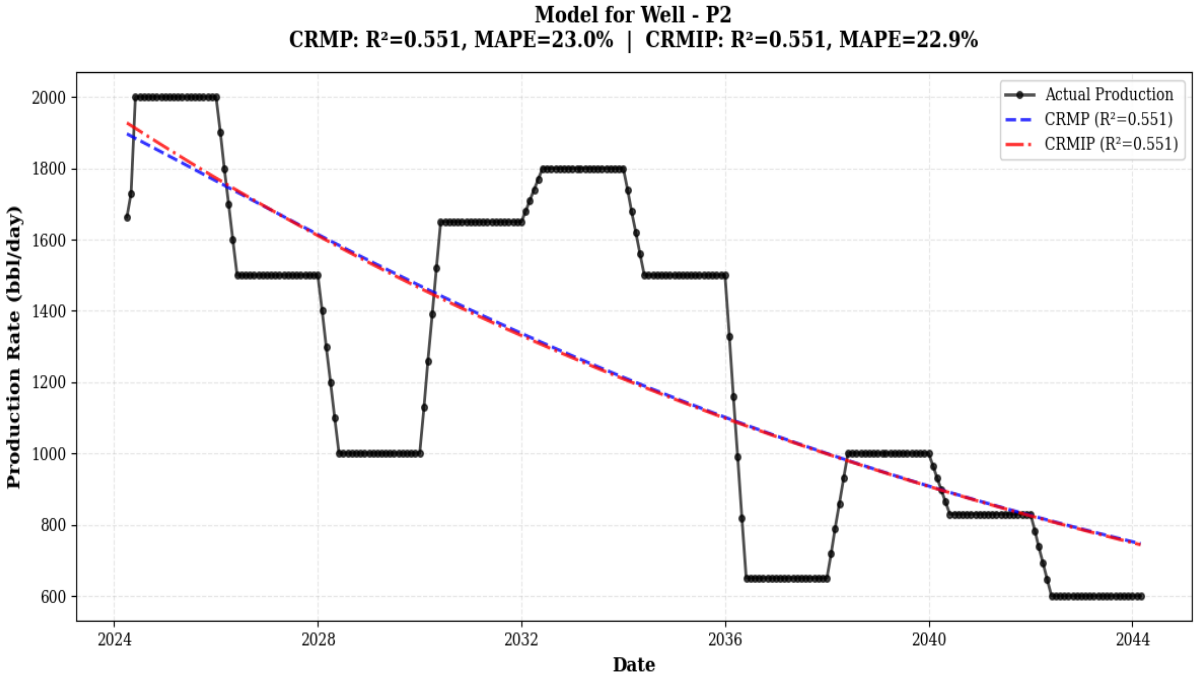

Figure 16 (b)

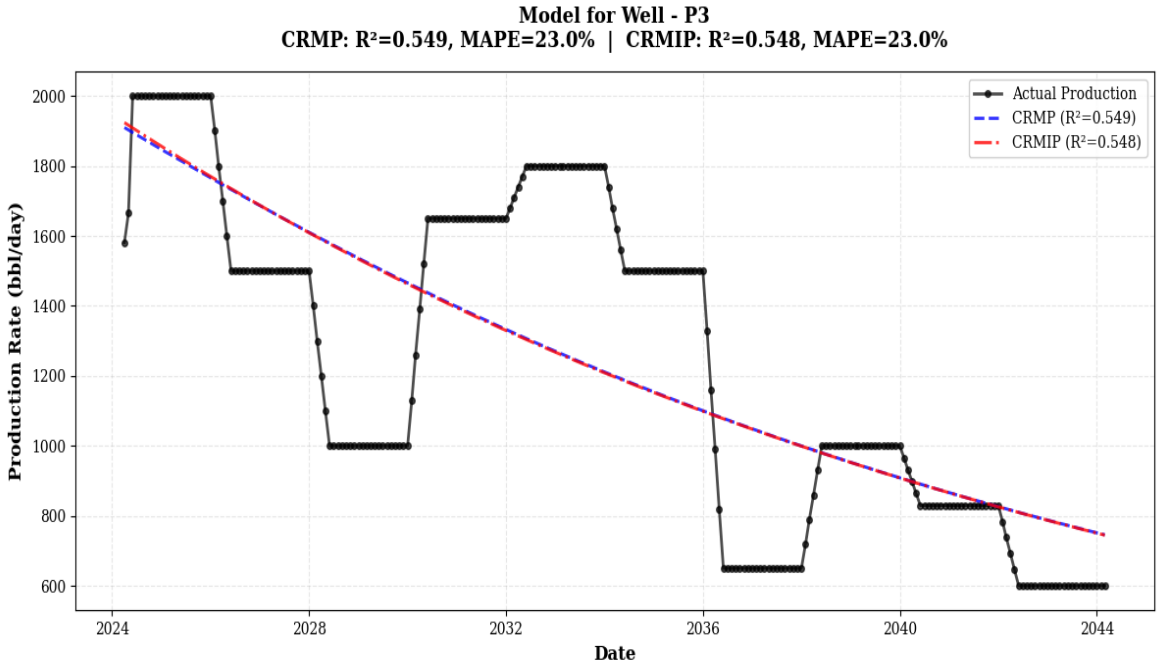

Figure 16 (c)
Figure 16. Prediction CRM after CO_2 injection

Both models (CRMP and CRMIP) show nearly identical performance across all three wells, with very small metric differences. The step-wise patterns in actual production data indicate operational changes or well interventions that affected production rates throughout the observation period (Fu et al., 2022). These results align with the established understanding that capacitance-resistance models are semi-analytical methods designed to estimate production rates based on historical production and injection data using material balance and signal correlations between injectors and producers (Fu et al., 2022.

The interwell connectivity coefficients and time constants presented in Tables 2-4 were derived from historical waterflooding data using CRM. These parameters define the baseline geological connectivity for the reservoir, representing the preferential flow paths established by the static permeability field and reservoir architecture. Although the absolute values of connectivity may evolve during CO_2 injection due to changes in fluid mobility and potential geochemical reactions, the relative connectivity hierarchy between well pairs is expected to remain stable. The most conductive pathways identified during waterflooding (I1→P2) are likely to become the dominant conduits for CO_2 flow, resulting in early breakthrough in the same wells. Furthermore, the relatively uniform time constants observed during waterflooding indicate a well-connected reservoir compartment, providing a calibrated reference for pressure transmission dynamics. This baseline connectivity is essential for initializing and interpreting the more complex CO_2 injection forecast, as it grounds the predictive models in the historically validated flow geometry of the field.

It is important to note that this baseline connectivity assumes no significant alteration of the pore structure during CO_2 injection. In reality, dynamic processes such as CO_2-induced wettability alteration and mineral dissolution/ precipitation could modify the effective permeability along flow paths over time. The simulation results in Figure 12, the oil saturation map indicates uneven sweep, which may be a consequence of both this static baseline heterogeneity and is amplified by these dynamic effects. Therefore, the waterflooding-based connectivity should be interpreted as the initial condition for the CO_2 flood. The forecasted production profiles and the updated connectivity analysis after the CO_2 injection period, as shown in Tables 6 - 8, reflect how these initial pathways

influence the eventual CO_2 sweep pattern and where dynamic effects might have played a role.

The interwell connectivity parameters derived from waterflooding history (Tables 2 – 4) serve as a geologically grounded baseline for initializing CO_2 injection forecasts. This approach is justified because connectivity during waterflooding reflects the static permeability field and reservoir architecture, which remain unchanged at the onset of CO_2 injection. While fluid mobility and relative permeability alter during CO_2 flooding, the preferential flow paths identified during waterflooding are expected to dominate early CO_2 migration. This assumption is supported by the consistent time constants observed (≈30 days), indicating a stable pressure transmission framework. Consequently, waterflooding connectivity provides a physically interpretable starting point for forecasting, from which dynamic effects such as miscibility, swelling, and mobility contrasts can be superimposed to predict CO_2-specific responses (Fu et al., 2022.

Table 6. Interwell Connectivity and Time Constant after CO_2 Injection CRMP

Production Well	Injection Well		Time Constant (τ) Days
	I1	I2	
P1	0.000036	0.000030	1358.83
P2	0.000228	0.000030	1464.74
P3	0.000063	0.000052	1554.69

Table 7. Interwell Connectivity after CO_2 Injection CRMIP

Production well	Injection well	
	I1	I2
P1	0.000038	0.000046
P2	0.000063	0.000004
P3	0.000054	0.000066

Table 8. Time Constant after CO_2 Injection CRMIP

Production well	Injection well	
	I1	I2
P1	915.83	915.66
P2	927.17	926.26
P3	921.60	921.52

The interwell connectivity analysis, Tables 6 - 7, shows distinct communication patterns between injection and production wells after CO_2 injection in both CRMP and CRMIP models. In the CRMP model in Table 6, interwell connectivity values range from 0.000030 to 0.000063, with P3 having the highest connectivity (0.000063 for I1 and 0.000052 for I2). The CRMIP model (Table 7) demonstrates similar magnitudes but different distribution patterns, with P2 exhibiting the strongest response to I1 (0.000063), while P1 shows higher connectivity to I2 (0.000046).

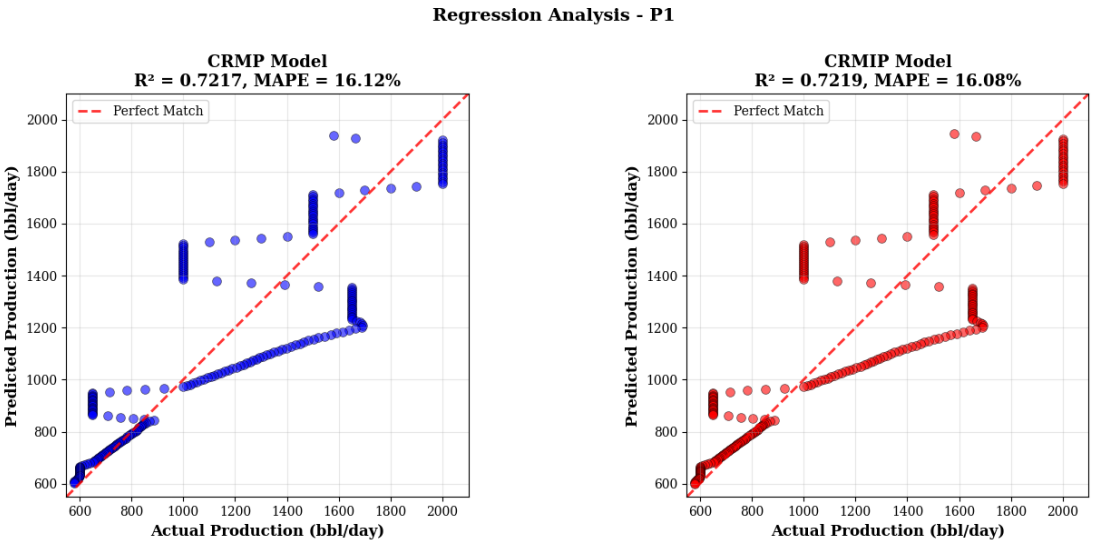

Figure 17. Comparison regression plot after CO_2 injection for Well Production (P1, P2, and P3)

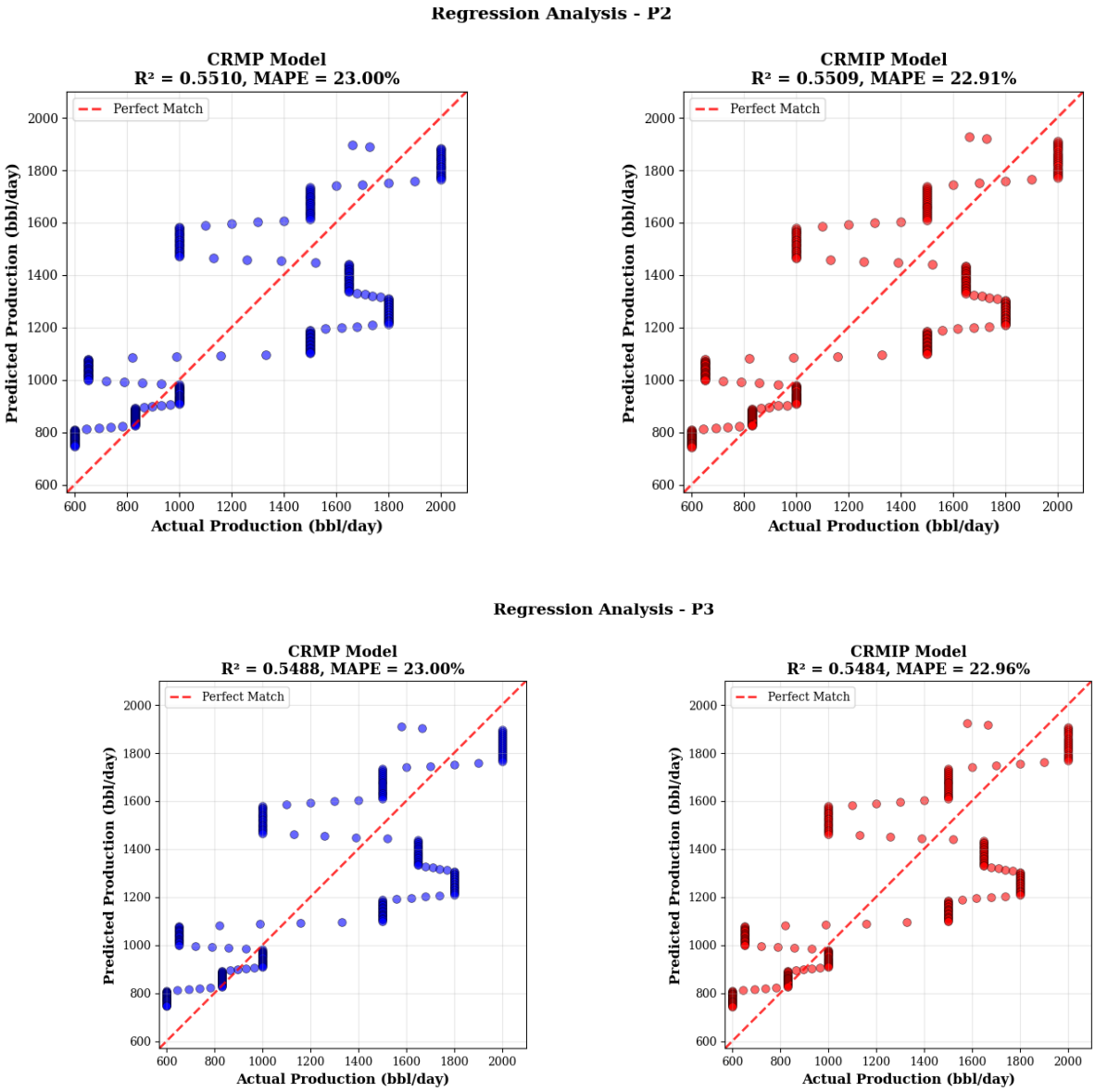

Time constant analysis shown in Table 8 indicates relatively consistent reservoir response times across all wells, ranging from 915.66 to 927.17 days. The uniformity of time constants (approximately 920 days) suggests homogeneous reservoir properties and similar fluid flow characteristics between injection and production wells. P2 exhibits the longest time constant (927.17 days for I1), indicating a slightly slower pressure response, whereas P1 shows the fastest response (915.66 days for I2). These time constants reflect the reservoir's capacity to transmit pressure signals and provide insights into CO_2 migration patterns and sweep efficiency in the enhanced oil recovery process. This analysis aligns with established research on interwell connectivity modeling (W. Wang et al., 2017 and CO_2 injection dynamics for enhanced oil recovery.

Figure 17 presents the regression analysis comparing CRMP and CRMIP model predictions against actual production data for wells P1, P2, and P3 after CO_2 injection. Well, P1 exhibits superior predictive performance with R^2 = 0.7217 (CRMP) and R^2 = 0.7219 (CRMIP), both achieving MAPE of approximately 16%. The data points demonstrate strong alignment with the perfect match line across the entire production range (600 - 2000 bbl/day), indicating reliable model calibration and accurate capture of production dynamics under CO_2-EOR conditions (Emera & Kalantari Dahaghi,

2025. Wells P2 and P3 show moderate predictive accuracy with lower R^2 values around 0.55 and higher MAPE values of approximately 23%. Both wells display similar scatter patterns with notable deviations from the perfect match line, particularly in the intermediate production range (1000 - 1600 bbl/day). This increased scatter suggests more complex reservoir responses to CO_2 injection, potentially due to heterogeneous fluid displacement patterns, variable CO_2 breakthrough timing, or localized reservoir compartmentalization (H. S. Lee et al., 2021).

Figure 18 illustrates the three-dimensional interwell connectivity map after CO_2 injection, revealing the spatial relationships and flow communication between injection and production wells (Ye et al., 2025). The visualization demonstrates distinct connectivity patterns, with P1 centrally positioned and receiving strong contributions from both I1 and I2, consistent with its superior regression performance ($R^2 > 0.72$) (Ye et al., 2025). Production wells P2 and P3, located in the western and northern regions, respectively, exhibit preferential connectivity to specific injectors based on spatial proximity and reservoir geometry (Sheng et al., 2021).

Connectivity pathways, indicated by directional arrows, show that I1 has a stronger influence over the western production zone (P2-P3), while I2 has more distributed connectivity across the field (Wei et al., 2025). The three-dimensional representation incorporates depth variations, suggesting potential gravitational segregation effects on CO_2 distribution (Wei et al., 2025).

This spatial connectivity analysis corroborates the interwell connectivity coefficients presented in Tables 6-7, providing geometric context for the observed flow patterns (Ye et al., 2025). The network topology confirms effective reservoir sweep by CO_2 injection. However, varied connectivity strengths explain the differential production responses observed in the regression analysis (Wei et al., 2025).

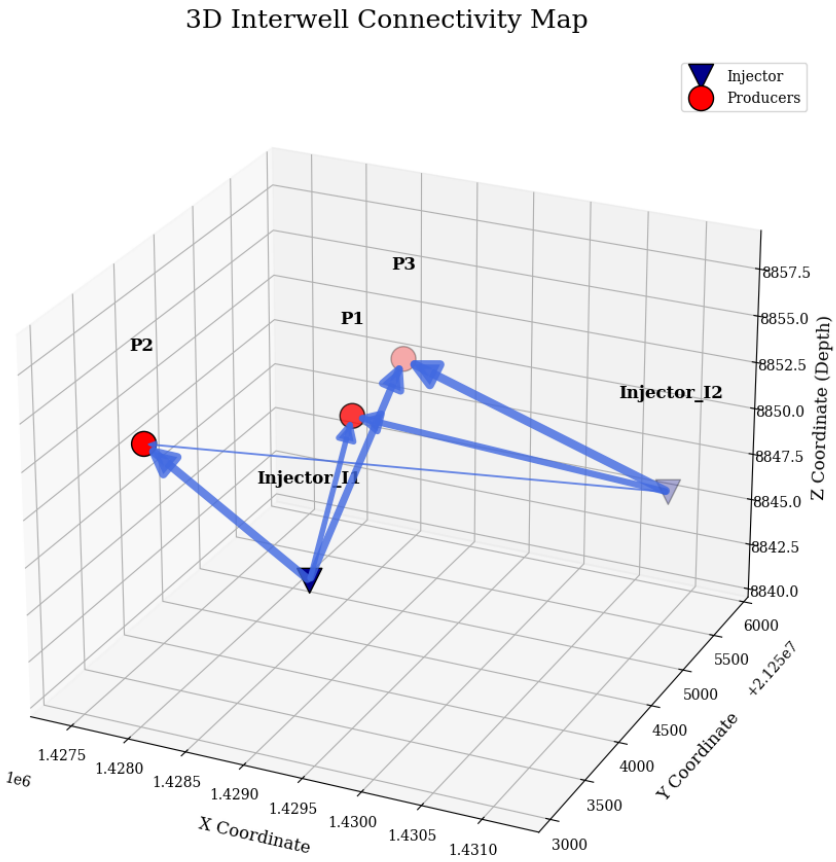

Figure 18. 3D interwell connectivity after CO_2 Injection

Figure 19 shows the Random Forest algorithm performance for production forecasting across all three wells following CO_2 injection (D. Fan et al., 2025). The machine learning approach demonstrates superior predictive accuracy compared to conventional CRM methods, with R^2 values ranging from 0.91 to 1.00 and MAPE below 2.5%. Well, P1 achieves near-perfect prediction (R^2 = 1.00, MAPE = 0.93%), with history matching showing excellent alignment between actual and predicted production throughout the 20-year forecast period. Well P2 exhibits similarly strong performance (R^2 = 0.99, MAPE = 1.88%), successfully capturing production variability and decline trends (Z. Fan et al., 2024). Well, P3 shows slightly reduced but still robust accuracy (R^2 = 0.91, MAPE = 2.50%), with minor deviations during production transition phases (D. Fan et al., 2025). The regression plots confirm a tight correlation between predicted and actual values across the entire production range (600-2000 bbl/ day), with minimal scatter compared to CRMP/ CRMIP models (Z. Fan et al., 2024).

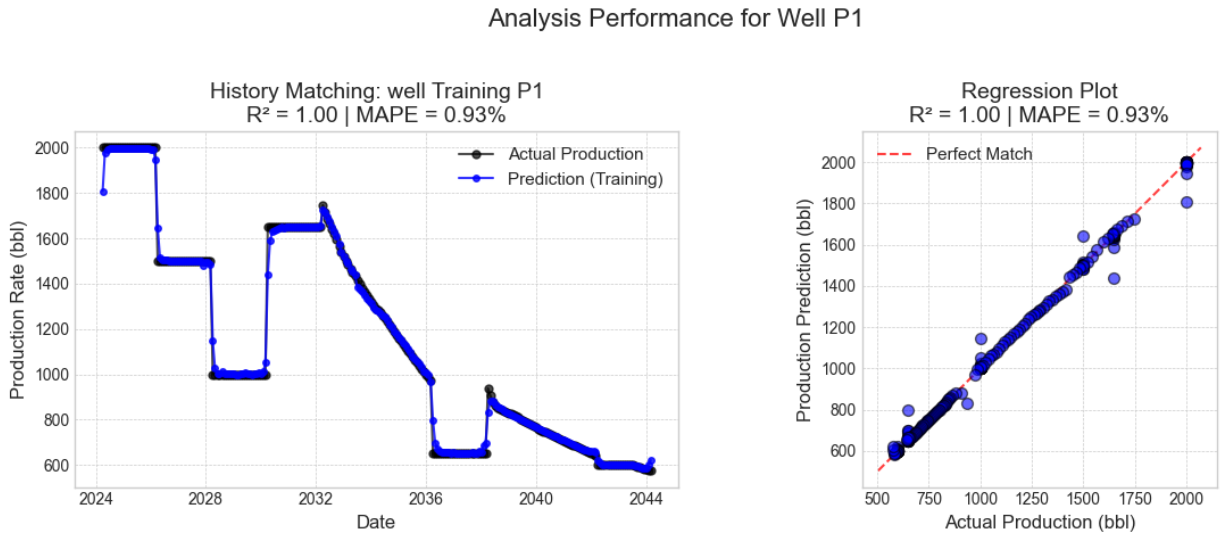

Figure 19 (a)

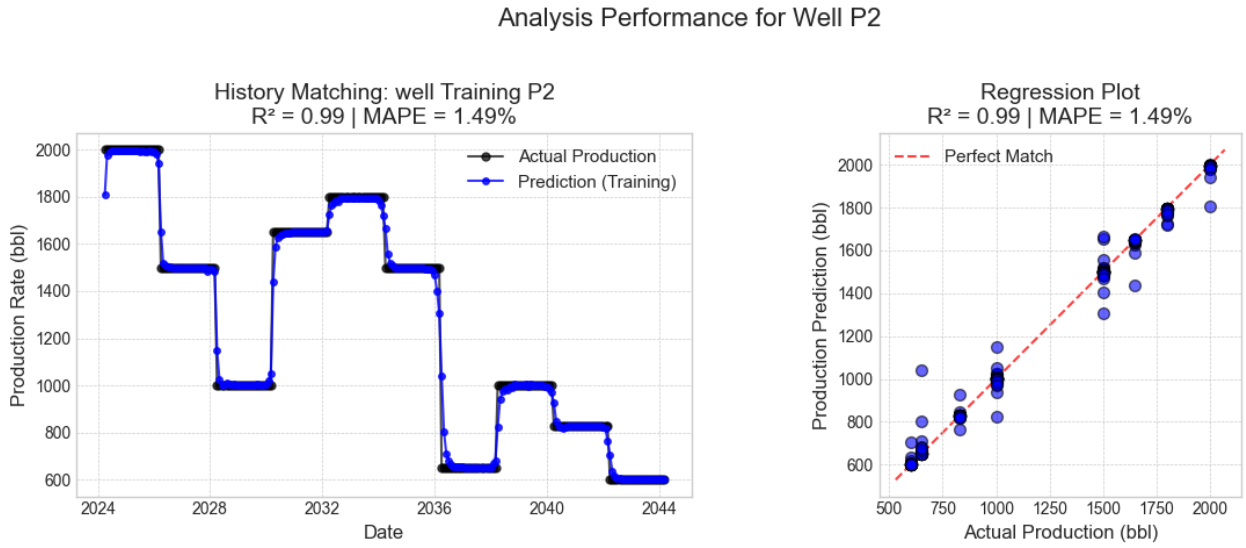

Figure 19 (b)

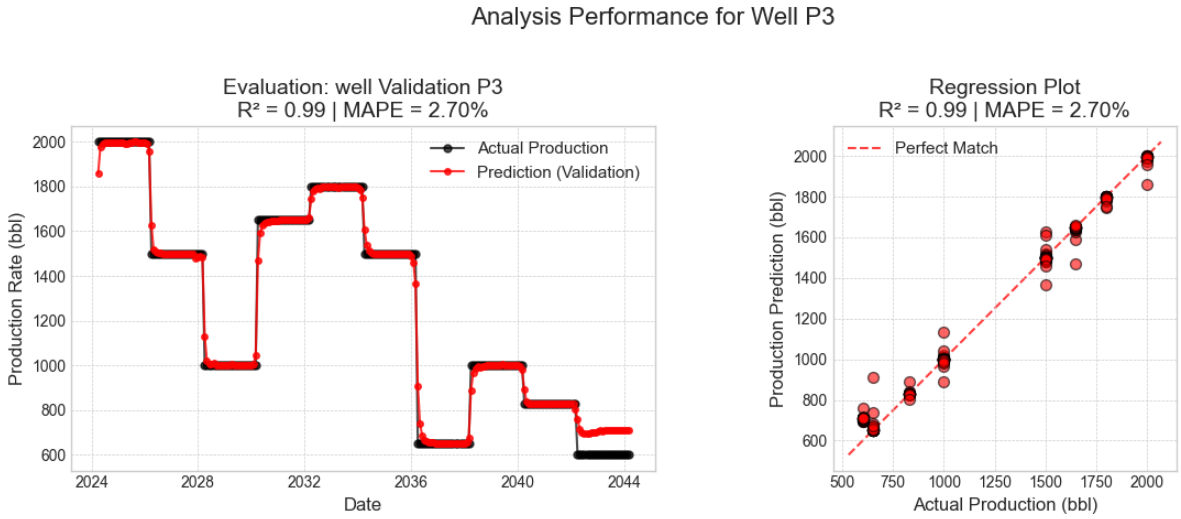

Figure 19 (c)
Analysis Random Forest for Well Production after CO_2 injection (P1, P2, and P3)

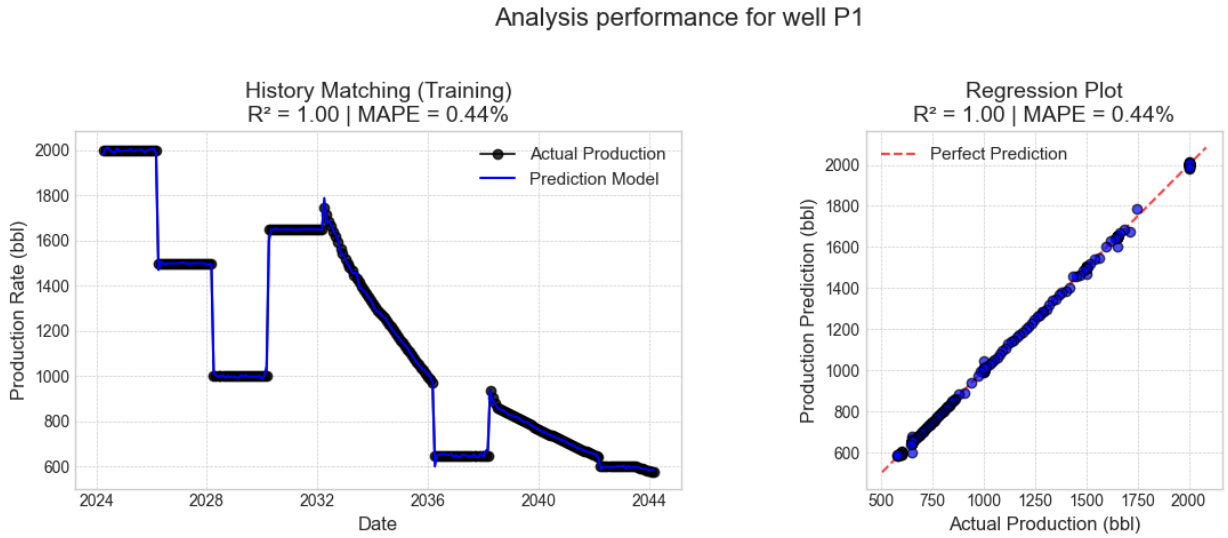

Figure 20 (a)

Figure 20 shows that the XGBoost algorithm performance for production forecasting following CO_2 injection, demonstrating exceptional predictive accuracy across all production wells (D. Fan et al., 2025). The model achieves near-perfect predictions with R^2 values of 0.99-1.00 and remarkably low MAPE ranging from 0.44% to 2.24%, representing the best performance among all evaluated methods (Xie et al., 2021). Well P1 exhibits the highest accuracy (R^2 = 1.00, MAPE = 0.44%), with history matching showing precise alignment between actual and predicted production throughout the 20-year forecast horizon, accurately capturing stepwise decline patterns (D. Fan et al., 2025).

Well, P2 demonstrates similarly outstanding performance (R^2 = 1.00, MAPE = 0.60%), successfully modeling complex production fluctuations and transitions. Well, P3 shows robust accuracy (R^2 = 0.99, MAPE = 2.24%), though with marginally higher prediction errors during specific operational phases. The regression plots confirm tight correlations over the entire production range (600-2000 bbl/day), with minimal scatter compared to both Random Forest and conventional CRM approaches.

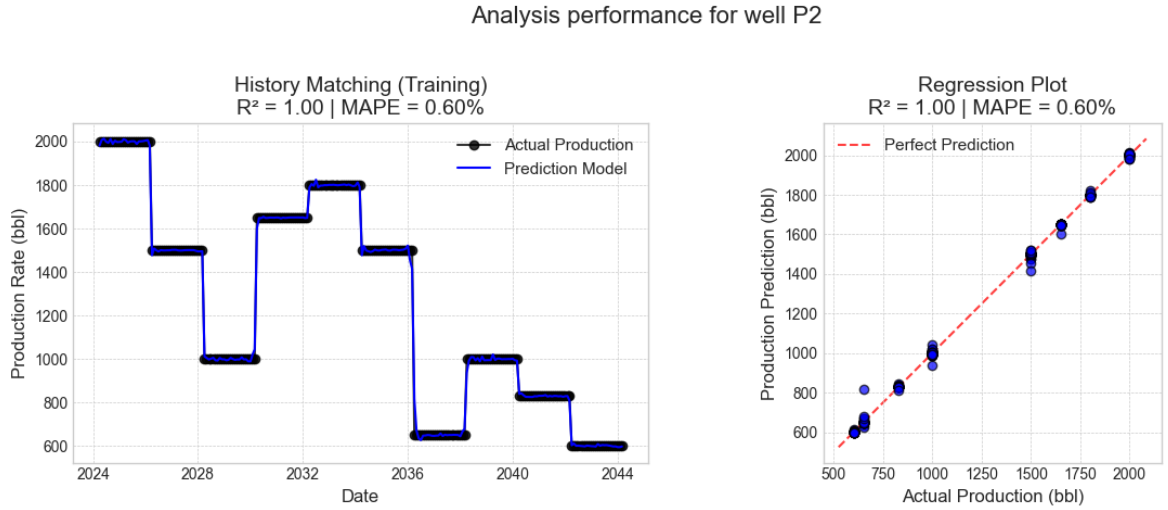

Figure 20 (b)

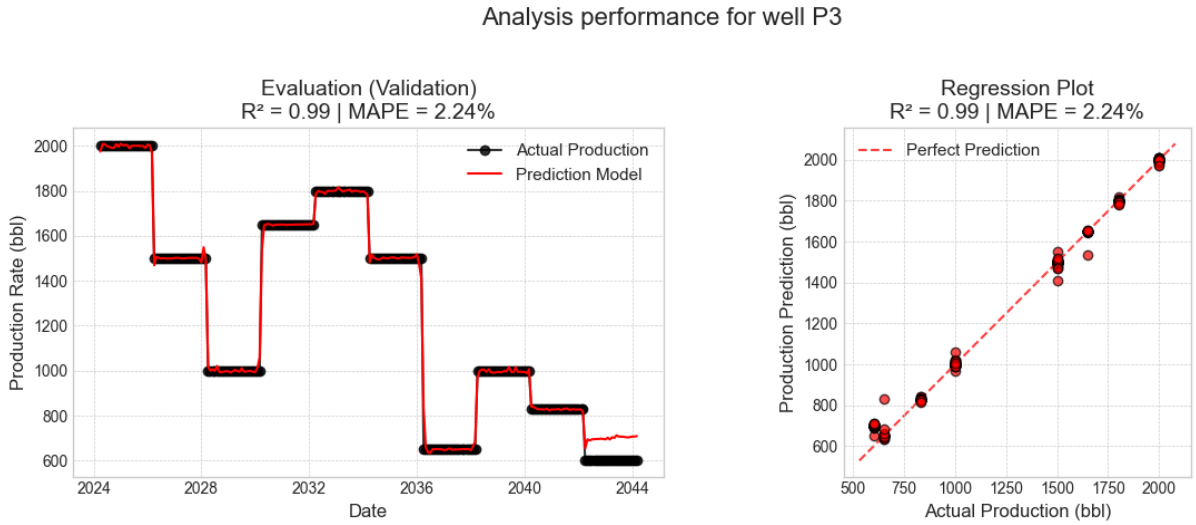

Figure 20 (c)

Model performance during waterflooding : establishing the baseline

During the waterflooding phase, the Capacitance-Resistance models (CRMP and CRMIP) demonstrated adequate performance in matching historical data, with R^2 values ranging from 0.72 to 0.79 and Mean Absolute Percentage Error (MAPE) below 23%. This performance indicates that this simplified physics-based approach is capable of capturing basic linear production trends and providing valuable qualitative insights into inter-well connectivity and reservoir time constants (Gumiere et al., 2020).

However, the still significant error rate reveals the limitations of CRM in modeling more complex production fluctuations. In contrast, machine learning models show a dramatic leap in accuracy (Makhotin & Orlov, 2022). The Random Forest algorithm achieved an R^2 of approximately 0.98 with a MAPE of 6%, while XGBoost demonstrated exceptional performance with near-perfect accuracy (R^2 between 0.99 and 1.00, MAPE 0.44 – 2.24%) on both training and validation data (Khanal, 2022). The absolute superiority of ML at this stage proves its superior ability to learn the non-linear patterns inherent in waterflooding dynamics (D. Fan et al., 2025) while also setting a high-performance baseline for evaluation in more complex scenarios.

Table 9. Comparative performance of CRM and machine learning models for production forecasting

Scenario	Model	Target Phase	R^2	MAPE
Waterflooding	CRMP/CRMIP	History Matching	0.72 – 0.79	< 23%
	Random Forest	History Matching	~0.98	~6%
	XGBoost	History Matching	0.99 – 1.00	0.44% - 2.24%
CO_2 Injection	CRMP/CRMIP	20-Year Forecast	0.55 – 0.72	16% - 23%
	Random Forest	20-Year Forecast	0.91 – 1.00	0.93% - 2.50%
	XGBoost	20-Year Forecast	0.99 – 1.00	0.44% - 2.24%

The predictive challenge of CO_2 enhanced oil recovery

The transition to the CO_2 injection scenario tests the resilience of each model in dealing with non-linear multi-phase flow dynamics (D. Fan et al., 2025). Here, the fundamental limitations of the CRM approach become very apparent. The predictive performance of CRMP and CRMIP declined significantly, with R^2 falling to the range of 0.55 – 0.72 and MAPE remaining high at 16–23%. This decline directly reflects the inability of the linear assumptions and fixed parameters in CRM to represent complex processes such as CO_2-oil miscibility, dynamic saturation changes, and fluid mobility alterations (Hamadi et al., 2023). The "step-wise" production patterns resulting from the simulations, which reflect CO_2 breakthrough and operational responses, fail to be captured by these continuous analytical formulations. Meanwhile, machine learning models showed impressive robustness (Du et al., 2024). Both Random Forest and XGBoost maintained high accuracy in 20-year long-term forecasting (Gao et al., 2023). Random Forest achieved R^2 between 0.91 and 1.00 with MAPE below 2.5%, while XGBoost again recorded the best performance with near-perfect consistency (R^2 0.99 – 1.00, MAPE 0.44 – 2.24%) (Gao et al., 2023).

The ability of these ensemble algorithms to maintain high precision - even when trained on waterflooding data and predicted on CO_2-induced reservoir response - confirms that they are not merely memorizing data, but have learned a fundamental representation that can be generalized from reservoir behavior, including complex fluid interactions (Li et al., 2022).

Synthesis and implications for forecasting practice

This comparative analysis leads to obvious conclusions regarding the suitability of each model's application. CRM is a crucial technique for physically interpretable initial connectivity analysis in flood control, whereas ML provides unmatched predictive precision for operational optimization. However, for forecasting CO_2-EOR performance, the superiority of machine learning is absolute (Gao et al., 2023). The degradation of CRM performance under complex non-linear flow conditions limits its usefulness as a standalone forecasting tool. In contrast, the robustness and high accuracy of ML models, particularly XGBoost, make them the preferred methodology for reliable planning and decision-making in CCUS projects (Gao et al., 2023). As a result, the integrated framework proposed in this study, where CRM provides an initial physical understanding of reservoir connectivity that is then enriched and operationalized by the predictive capabilities of machine learning, represents a comprehensive and robust approach to optimizing EOR implementation in heterogeneous reservoirs (Li et al., 2022).

CONCLUSION

This study successfully establishes a robust predictive framework for CO_2-EOR performance forecasting in heterogeneous reservoirs. The analysis demonstrates that while Capacitance-Resistance Models provide valuable, physically interpretable insights into baseline interwell connectivity, their predictive accuracy is fundamentally limited under the complex, non-linear dynamics of CO_2 flooding. In contrast,

ensemble machine learning algorithms, particularly XGBoost, demonstrate remarkable capability in capturing these complex interactions, achieving exceptional predictive accuracy (R^2 up to 1.00, MAPE as low as 0.44%) that far surpasses conventional CRM methods. The research quantitatively establishes the critical fluid-mechanistic parameters governing CO_2-EOR success in the Volve Field, including a Minimum Miscibility Pressure of 3299.68 psi and an oil Swelling Factor of 1.19.

These parameters provide the physical foundation for the substantial incremental recovery of 6.35 MMSTB achieved in the 20-year CO_2 injection forecast, representing a 67.7% improvement over conventional waterflooding. However, the analysis also reveals that the very mechanisms enabling this enhanced recovery—miscibility and swelling—are inherently pressure-dependent, which amplifies the effects of reservoir heterogeneity and leads to uneven sweep efficiency and early CO_2 breakthrough. The integrated framework combines physics-based models with machine learning to provide a comprehensive approach to CO_2-EOR forecasting. It provides not only accurate production predictions but also deeper insights into evolving connectivity patterns and displacement mechanisms. This dual capability enables better-informed operational decision-making and strategy optimization for CCUS implementation in complex, heterogeneous reservoirs, ultimately contributing to both enhanced hydrocarbon recovery and effective carbon management.

ACKNOWLEDGEMENT

The authors would like to thank the Laboratory of Petroleum Engineering Study Program, the Engineering Faculty, Islamic University of Riau, and the PT. Pertamina Hulu Rokan.

GLOSSARY OF TERM

Unit	Definition	Symbol
CRM	Capacitance Resistance Model	
DCA	Decline Curve Analysis	
I_1, I_2	Injection Wells 1 and 2	
MAPE	Mean Absolute Percentage Error	%
P1, P2, P3	Production Wells 1,2, and 3	
XGBOOST	eXtreme Gradient Boosting	
R^2	Coefficient Determination	
RF	Recovery Factor	%
CCUS	Carbon, Capture, Utilization, and Storage	
EOR	Enhanced Oil Recovery	
CO_2	Carbon Dioxide	Ton/Day
MMSCF	Million Standard Cubic Feet	
MMSTB	Million Stock Tank Barrels	
MMP	Minimum Miscibility Pressure	
f_ij	Coefficient Connevtivity injection Producer	
τ	Time Constant	Day

REFERENCES

Ahmed, T. (2007). Reservoir Engineering Handbook. In Cardiovascular Imaging (Vol. 27, Issue 7). https://doi.org/10.1016/B978-1-4160-5009-4.50004-2

Alam, M. M. M., Hassan, A., Mahmoud, M., Sibaweihi, N., & Patil, S. (2022). Dual Benefits of Enhanced Oil Recovery and CO2 Sequestration: The Impact of CO2 Injection Approach on Oil Recovery. Frontiers in Energy Research, 10(April), 1–9. https://doi.org/10.3389/fenrg.2022.877212

Arps. (n.d.). Decline_Curve_Analysis.pdf.

Asnawi, M. F., Bisono, H. H., Megantara, M. A., & Kusrini, K. (2024). Aplikasi Prediksi Banjir Menggunakan Algoritma XGBoost Berbasis Website. Journal of Economic, Management, Accounting and Technology, 7(2), 379–389. https://doi.org/10.32500/jematech.v7i2.7644

Chavez-Rodriguez, M. F., Szklo, A., & de Lucena, A. F. P. (2015). Analysis of past and future oil production in Peru under a Hubbert approach. Energy Policy, 77(May 2021), 140–151. https://doi.org/10.1016/j.enpol.2014.11.028

Chicco, D., Warrens, M. J., & Jurman, G. (2021). The coefficient of determination, R-squared, is more informative than SMAPE, MAE, MAPE, MSE, and RMSE in regression analysis evaluation. PeerJ Computer Science, 7, 1–24. https://doi.org/10.7717/PEERJ-CS.623

De Holanda, R. W., Gildin, E., Jensen, J. L., Lake, L. W., & Shah Kabir, C. (2018). A state-of-the-art literature review on capacitance resistance models for reservoir characterization and performance forecasting. Energies, 11(12). https://doi.org/10.3390/en11123368

Du, X., Salasakar, S., & Thakur, G. (2024). A Comprehensive Summary of the Application of Machine Learning Techniques for CO2-Enhanced Oil Recovery Projects. Machine Learning and Knowledge Extraction, 6(2), 917–943. https://doi.org/10.3390/make6020043

Emera, R., & Kalantari Dahaghi, A. (2025). Maximizing conventional oil recovery and carbon mitigation: an artificial intelligence-driven assessment and optimization of carbon dioxide enhanced oil recovery with physics-based dimensionless type curves. Frontiers in Energy Research, 13(March), 1–20. https://doi.org/10.3389/fenrg.2025.1478473

Erfando, T., & Khariszma, R. (2023). Sensitivity Study of the Effect of Polymer Flooding Parameters To Improve Oil Recovery Using X-Gradient Boosting Algorithm. Journal of Applied Engineering and Technological Science, 4(2), 873–884. https://doi.org/10.37385/jaets.v4i2.1871

Fajrul Haqqi, M., Saroji, S., & Prakoso, S. (2023). An implementation of the XGBoost algorithm to estimate effective porosity on well log data. Journal of Physics: Conference Series, 2498(1). https://doi.org/10.1088/1742-6596/2498/1/012011

Fan, D., Lai, S., Sun, H., Yang, Y., Yang, C., Fan, N., & Wang, M. (2025). Review of Machine Learning Methods for Steady State Capacity and Transient Production Forecasting in Oil and Gas Reservoirs. Energies, 18(4), 1–25. https://doi.org/10.3390/en18040842

Fan, Z., Liu, X., Wang, Z., Liu, P., & Wang, Y. (2024). A Novel Ensemble Machine Learning Model for Oil Production Prediction with Two-Stage Data Preprocessing. Processes, 12(3). https://doi.org/10.3390/pr12030587

Fang, P., Zhang, Q., Zhou, C., Yang, Z., Yu, H., Du, M., Chen, X., Song, Y., Wang, S., Gao, Y., Dou, Z., & Cao, M. (2024). Chemical-Assisted CO2 Water-Alternating-Gas Injection for Enhanced Sweep Efficiency in CO2-EOR. Molecules, 29(16), 1–31. https://doi.org/10.3390/molecules29163978

Fu, L., Zhao, L., Chen, S., Xu, A., Ni, J., & Li, X. (2022). A Prediction Method for Development Indexes of Waterflooding Reservoirs Based on Modified Capacitance–Resistance Models. Energies, 15(18). https://doi.org/10.3390/en15186768

Gao, M., Liu, Z., Qian, S., Liu, W., Li, W., Yin, H., & Cao, J. (2023). Machine-Learning-Based Approach to Optimize CO2-WAG Flooding in Low Permeability Oil Reservoirs. Energies, 16 (17). https://doi.org/10.3390/en16176149

Gumiere, S. J., Camporese, M., Botto, A., & Lafond, J. A. (2020). Machine Learning vs Physics-Based Modeling for Real-Time Irrigation Management. April. https://doi.org/10.3389/frwa.2020.00008

Hamadi, M., Mehadji, T. El, Laalam, A., Zeraibi, N., Tomomewo, O. S., Ouadi, H., & Dehdouh, A. (2023). Prediction of Key Parameters in the Design of CO 2 Miscible Injection via the Application of Machine Learning Algorithms. 1905–1932. https://doi.org/https://doi.org/10.3390/ eng4030108

Hidayat, F., & Astsauri, T. M. S. (2021). Applied random forest for parameter sensitivity of low-salinity water injection (LSWI). https://doi.org/10.1016/j.aej.2021.06.096

Jiashun Luo. (2022). Effect of Reservoir Heterogeneity on CO2 Flooding in Tight Oil Reservoirs. https://doi.org/10.3390/en15093015

Khanal, A. (2022). Physics-Based Proxy Modeling of CO 2 Sequestration in Deep Saline Aquifers.

https://doi.org/https://doi.org/10.3390/en15124350

Khurshid, I., & Afgan, I. (2021). Geochemical investigation of CO2 injection in oil and gas reservoirs of the Middle East to estimate the formation damage and related oil recovery. Energies, 14(22). https://doi.org/10.3390/en14227676

Kristanto, D., Hariyadi, Pramudiohadi, E. W., Kurniawan, A., Nursidik, U. S., Asmorowati, D., Widiyaningsih, I., & Cahyaningtyas, N. (2025). Optimization of CO2 Injection Through Cyclic Huff and Puff to Improve Oil Recovery. Scientific Contributions Oil and Gas, 48(2), 53–67. https://doi.org/10.29017/scog.v48i2.1659

Lee, H. S., Cho, J. H., Lee, Y. W., & Lee, K. S. (2021). Compositional modeling of impure CO2 injection for enhanced oil recovery and CO2 storage. Applied Sciences (Switzerland), 11 (17). https://doi.org/10.3390/app11177907

Lee, S., Bae, W., Permadi, A. K., & Park, C. (2023). Hydraulic Stimulation of Enhanced Geothermal System: A Case Study at Patuha Geothermal Field, Indonesia. International Journal of Energy Research, 2023. https:// doi.org/10.1155/2023/9220337

Li, H., Gong, C., Liu, S., & Xu, J. (2022). Applied Sciences Machine Learning-Assisted Prediction of Oil Production and CO 2 Storage Effect in CO 2 -Water-Alternating-Gas Injection (CO 2 - WAG). https://doi.org/https:// doi.org/10.3390/ app122110958

Makhotin, I., & Orlov, D. (2022). Machine Learning to Rate and Predict the Efficiency of Waterflooding for Oil Production. https:// doi.org/https:// doi.org/10.3390/en15031199

Moreno, G. A., & Lake, L. W. (2014). Input signal design to estimate interwell connectivities in mature fields from the capacitance-resistance model. Petroleum Science, 11(4), 563–568. https://doi.org/10.1007/s12182-014-0372-z

Núñez-lópez, V., & Moskal, E. (2019). Potential of CO 2 -EOR for Near-Term Decarbonization. 1(September). https://doi.org/10.3389/fclim.2019.00005

Orin, T. Z., Rahman, M. T., Islam, M. A., Alam, K. M. H., Mannafi, A. S. M., & Habib, K. (2025). Enhanced Oil Recovery through Carbon dioxide Injection: A Compositional Simulation Approach. Journal of Advanced Research in Applied Sciences and Engineering Technology, 49(1), 149 –160. https://doi.org/10.37934/araset.49.1.149160

Qiao, M., & Zhang, F. (2025). Rheological Properties of Crude Oil and Produced Emulsion from CO 2 Flooding. https://doi.org/10.3390/ en18030739

Ramadhan, R., Novriansyah, A., Erfando, T., Tangparitkul, S., Daniati, A., Permadi, A. K., & Abdurrahman, M. (2023). Heterogeneity Effect on Polymer Injection: a Study of Sumatra Light Oil. Scientific Contributions Oil and Gas, 46(1), 39–52. https://doi.org/10.29017/SCOG.46.1.1322

Rhamadhani, D. A., Saputri, E. E. D., & Sari, R. L. (2023). Forecasting Oil Production of Well 159-F-14H in the Volve Field Using a Machine Learning Model. Indonesian Journal of Artificial Intelligence and Data Mining, 7(1), 86. https://doi.org/10.24014/ijaidm.v7i1.24907

Salehian, M., & Çınar, M. (2019). Reservoir characterization using dynamic capacitance–resistance model with application to shut-in and horizontal wells. Journal of Petroleum Exploration and Production Technology, 9(4), 2811–2830. https://doi.org/10.1007/s13202-019-0655-4

Saraiva, T. A., Szklo, A., Lucena, A. F. P., & Chavez-Rodriguez, M. F. (2014). Forecasting Brazil's crude oil production using a multi-Hubbert model variant. Fuel, 115(2014), 24–31. https://doi.org/10.1016/j.fuel.2013.07.006

Shabani, A., Moosavi, M. S., Zivar, D., & Jahangiri, H. R. (2020). Data-driven technique for analyzing the injector efficiency in a waterflooding operation. Simulation, 96(8), 701–710. https:// doi.org/10.1177/0037549720923386

Shafiei, M., Kazemzadeh, Y., Escrochi, M., Cortés, F. B., Franco, C. A., & Riazi, M. (2024). OPEN A comprehensive review of direct methods to overcome the limitations of gas injection during the EOR process. Scientific Reports, 1–29. https://doi.org/10.1038/s41598-024-58217-1

Sheng, S., Duan, Y., Wei, M., Yue, T., Wu, Z., & Tan, L. (2021). Analysis of Interwell Connectivity of Tracer Monitoring in Carbonate Fracture-Vuggy Reservoir: Taking T-Well Group of Tahe

Oilfield as an Example. Geofluids, 2021. https://doi.org/10.1155/2021/5572902

Sugihardjo, O. (2009). Perubahan Sifat-Sifat Fluida Reservoir pada Injeksi CO 2. 43(1), 11–16. https://doi.org/https://doi.org/10.29017/LPMGB.43.1.122

Telmadarreie, A., & Trivedi, J. J. (2020). CO2 foam and CO2 polymer-enhanced foam for heavy oil recovery and CO2 storage. Energies, 13(21), 1–15. https://doi.org/10.3390/en13215735

Wang, D., Li, Y., Zhang, J., Wei, C., Jiao, Y., & Wang, Q. (2019). Improved CRM model for inter-well connectivity estimation and production optimization: Case study for karst reservoirs. Energies, 12(5). https://doi.org/10.3390/en12050816

Wang, W., Yao, J., Li, Y., & Lv, A. (2017). Research on carbonate reservoir interwell connectivity based on a modified diffusivity filter model. Open Physics, 15(1), 306–312. https://doi.org/10.1515/phys-2017-0034

Wei, J., Yan, Y., Chen, Y. J., Gao, M., Lv, W., Yu, H., Gao, Y., Chen, X., Tan, K., & Guan, Y. (2025). Experimental Study on the Sweep Patterns of CO2 Flooding in Reservoirs with Interlayer Heterogeneity. ACS Omega, 10(14), 14121–14137. https://doi.org/10.1021/acsomega.4c11327

Xie, Z., Feng, Q., Zhang, J., Shao, X., Zhang, X., & Wang, Z. (2021). Prediction of conformance control performance for cyclic-steam-stimulated horizontal well using the XGBoost: A case study in the Chunfeng heavy oil reservoir. Energies, 14 (23). https://doi.org/10.3390/en14238161

Ye, H., Deng, J., Ma, J., Zhang, K., Li, Y., Zhang, H., & Zhong, K. (2025). Interwell Connectivity Analysis Method Based on Injection–Production Data Time and Space Scale Coupling. Processes, 13(2), 1–13. https://doi.org/10.3390/pr13020373